Beam Physics Note
TRI-BN-20-08
May 15, 2020

The TRANSOPTR Model of the ISAC Drift Tube Linear Accelerator - Part I: Longitudinal Verification

Olivier Shelbaya

TRIUMF

Abstract: This note records the initial implementation of the ISAC Drift Tube Linac in the envelope code TRANSOPTR. As part of an effort to explore and map the vast set of longitudinal DTL tunes, a full model has been built using synthetic electric field distributions, generated in the Poisson solver Opera-2D, from detailed technical schematics of the as-built interdigital structure for each cavity of the accelerator. Exploiting TRANSOPTR's subsecond execution times means surveys of accelerated DTL output beam parameters versus cavity (V_s, ϕ) can be produced in a matter of minutes. Model computed output energy-phase curves at constant electric field amplitude are compared to on-line measurements using an oxygen beam, as part of a verification of model's longitudinal predictive power.

4004 Wesbrook Mall, Vancouver, B.C. Canada V6T 2A3 Tel: 604 222-1047 www.triumf.ca

Contents

1 Background: A Variable Energy Linac

This document records the TRANSOPTR implementation of the ISAC-DTL [1], a variable energy postaccelerator for low intensity radioisotope beams (RIB), whose design operating tank and buncher energies are listed in Table 1. Users of DTL beams are high energy nuclear physics experiments who by their nature constantly request different beam energies. This is achieved by sequential tuning of each tank and buncher to its design energy, up until the requested output energy is reached, with downstream tanks powered off. For example, a desired final output energy of 0.9 MeV/u would be achieved by setting up to Buncher-3 at design, with Tank-4 then being tuned to produce the desired output and Tank-5 off. It is important to stress that for the DTL, design energy is not the highest attainable tank energy. Instead, the design velocity for each tank produces a minimized increase in energy spread and bunch length, over the length of the machine.

Tank	E/A [MeV/u]
MEBT Rebuncher	0.153
IH Tank-1	0.238
Buncher-1	0.254
IH Tank-2	0.439
Buncher-2	0.461
IH Tank-3	0.781
Buncher-3	0.803
IH Tank-4	1.149
IH Tank-4	1.530

Table 1: Design output energies for the ISAC-DTL [2]. Note Tank-1 in practice is operated at 0.238 MeV/u while the reference quotes 0.236 MeV/u.

The mass-to-charge ratio for DTL accelerated beams by design is $2 \leq$ A/q ≤ 6. From electrodynamics, it follows that beams with the same A/q should have the same set of accelerating gradients (V_s) [3] and phases. For example, $^{20}Ne^{5+}$ and $^{16}O^{4+}$ should both have the same voltage gradient setpoints, while $^{20}Ne^{5+}$ and $^{12}C^{3+}$ will have gradients differing by a factor of 4/5, owing to the A/q difference. However, in terms of cavity phasing, there should be no difference since there is a unique time-of-flight profile between drift tubes and the injection beam velocity is unchanging.

Output DTL energy is measured using a 90° analyzing magnet coupled with a wire scanner (*the Harp*) [4], allowing operators to view the energy spectrum of the output bunch distribution. Operators power on the RF amplifiers at low amplitude to limit multipactoring behavior, which also produces minimal initial tank acceleration upon powerup. Tank setup or energy ramping proceeds when an operator manually tunes the parameter V_s while the energy spectrum is monitored on the Harp.

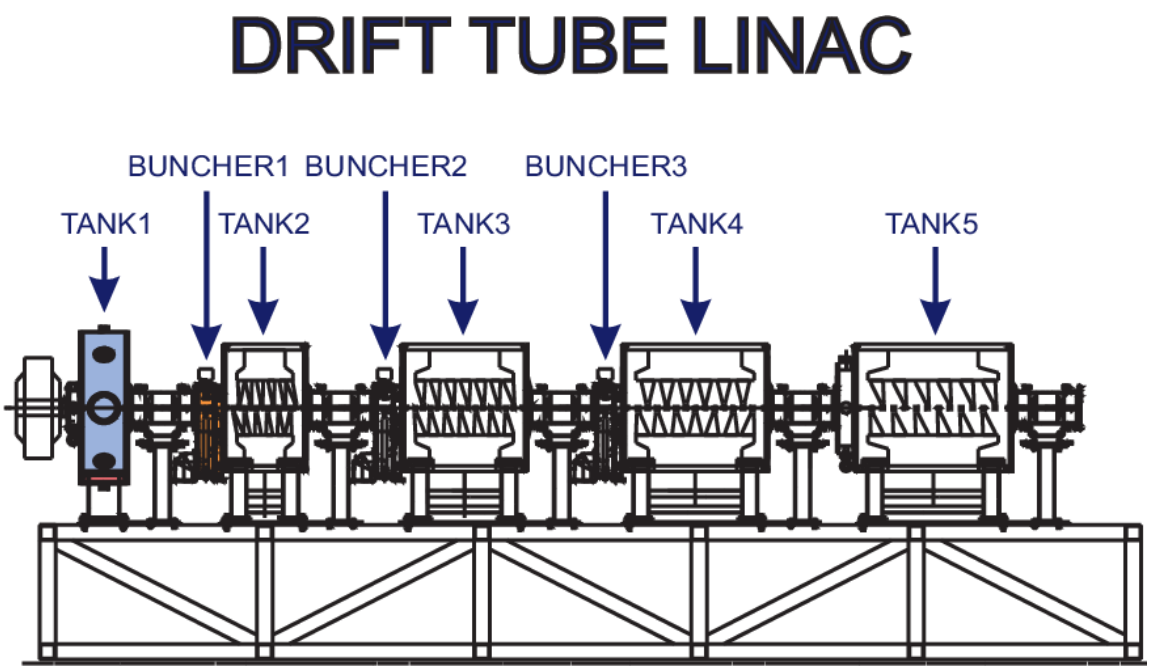

Figure 1: Overview of the ISAC Drift Tube Linac, an 106.08 MHz, separated function, interdigital H-mode heavy-ion linac. The quadrupole triplet assemblies, which provide transverse focusing, are interspersed between the tanks along the structure. Cutaway of tanks shows internal structure, where the IH drift tube supports can be seen attached to resonators at the top and bottom of each tank. The three bunchers are split-ring three-gap structures. Each buncher cavity is identical in dimension, while the gaps differ. Beam propagation occurs from left to right. Image courtesy M. Marchetto.

During the energy ramp, the RF phase is scanned to minimize the output beam energy spread [5]. This phase optimization is necessary to maintain beam transmission and keep the energy distribution visible on the Harp. Simultaneously, operators are also required to re-tune the quadrupole triplets and scale the HEBT quadrupole currents for the increased beam energy, not to mention continually tune the 90° magnet's field to keep beam visible on the diagnostic. The final DTL beam energy is computed from the current necessary to deflect beam at the HEBT1 station, using a BI parametrization of the magnet.

The above mentioned procedure is both time consuming and demanding on operators, due to the number of tasks that must be carried out simultaneously. In practice, it is not uncommon for an entire 8-hour shift to be consumed ramping the DTL to its full design energy. Further, the heavy procedural overhead produces a system which is prone to human error or oversight. The end result is that tuning the DTL is considered one of the most complex tasks to be carried out by operators.

However, from a physical standpoint, the intense procedural load is difficult to justify given the extreme reproducibility of the linac, in addition to the set of configurations for which the DTL is used in ISAC beam delivery. One would be justified in arguing that *a priori*, since it always ends up tuned within its nominal performance envelope and with a set of unchanging design energies, much of the initial setup procedure can be considerably reduced, by obtaining a full mapping of the energy-phase relation for each of the tanks and bunchers of the linac. This would allow operators to skip much of the ramping procedure, and go directly to the desired energy. Even better, if one can quickly model this, in a manner that agrees with the machine's behaviour, then much of this procedure can be automated and offloaded from the operators' plate altogether.

To date, the project to implement a full end-to-end model of the ISAC linac in TRANSOPTR has scrutinized OLIS and ILT [6, 7], added and benchmarked an optr-RFQ capability for the ISAC-RFQ [8] and also built and benchmarked the medium, high and superconducting energy beamlines [9, 10, 11]. An ISAC-II model of SCRF is, in parallel, underway [12, 13]. A tracking of global time was implemented in optr, to allow faithful modelling of inter-cavity time of flight effects [14] in all linac simulations.

Last year, an investigation of the DTL design tune found anomalies in quadrupole BI parametrizations and succeeded at achieving a high transmission on-line tune at tank-2 energy using model computed quadrupole setpoints. The Langevin-like BI parametrizations from that report [15] are used in the model.

And so, this document represents the laying of a cornerstone for the full TRANSOPTR model of the ISAC accelerator and with it the possibility of further developing the methods and principles of ISAC beam delivery. As the present DTL implementation is adaptable to the nascent HLA infrastructure at TRIUMF [16], the significance of this model and its capabilities should be evident.

2 On-Line DTL Energy-Phase Measurements

A comprehensive beam based measurement of the energy-phase output of each DTL tank and buncher was organized by the author in December 2017, using a $^{16}O^{4+}$ beam from the microwave source. Over a continuous 48 hour period, a team of volunteers assisted in performing these measurements, which provided a detailed mapping of output cavity energy versus cavity tuneable parameters (V_s, ϕ). The run plan and data acquisition protocol for this experiment are shown in Appendix A. The data, shown in Figures 2 and 3, preceded construction of the model and was consequently catalogued and stored until the present, where it is to be used for model verification, in Section 5.1.

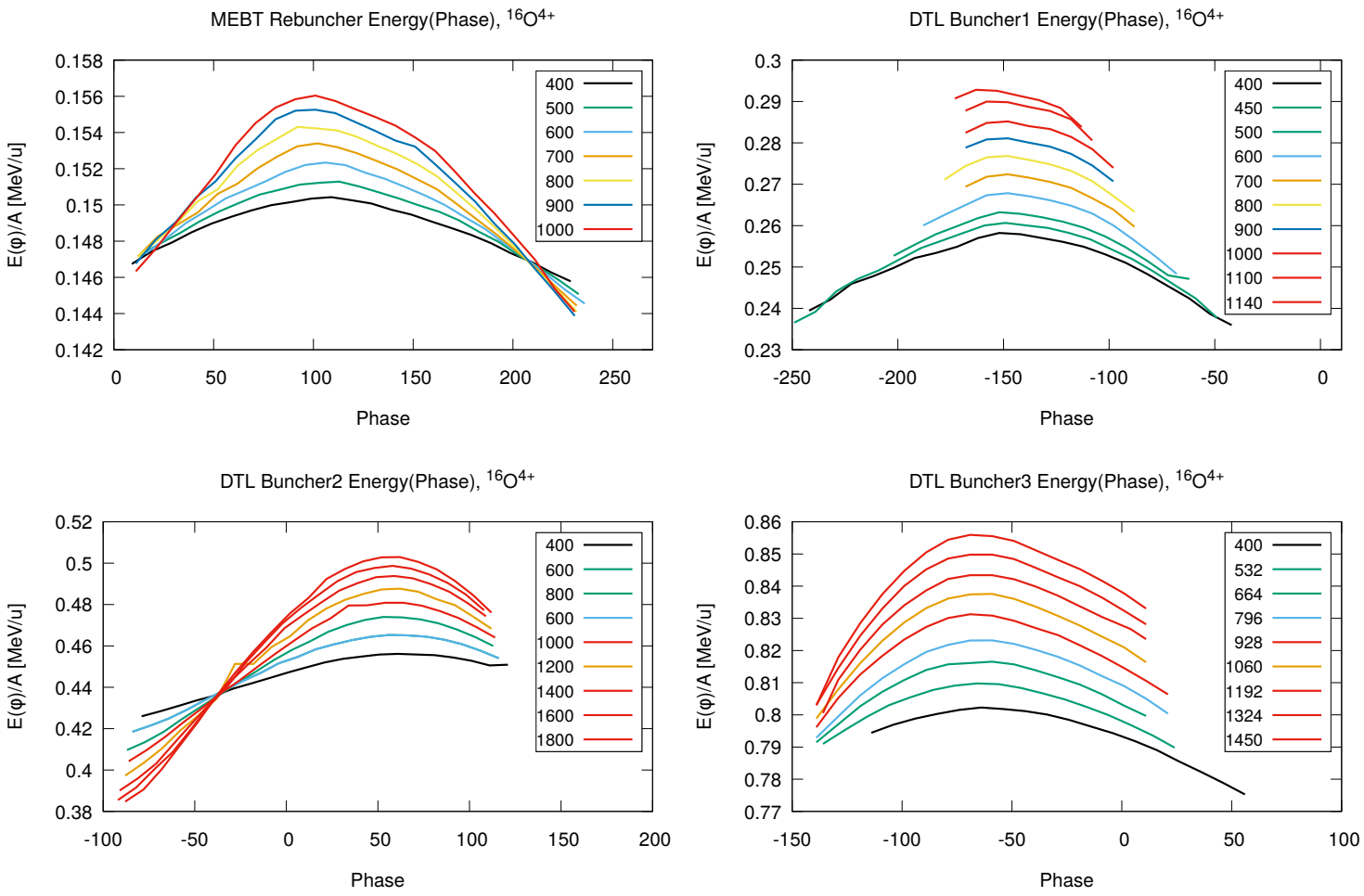

Figure 2: Energy-Phase lines for the MEBT Rebuncher, which precedes the ISAC-DTL, and of its bunchers, as measured with $^{16}O^{4+}$. Amplitude settings, as set by operators via EPICS, are shown in the legend for each plot. Each line shows the linac output for constant amplitude, implying constant on-axis electric field. The MEBT Rebuncher was mapped and is shown, though is not used in the present analysis.

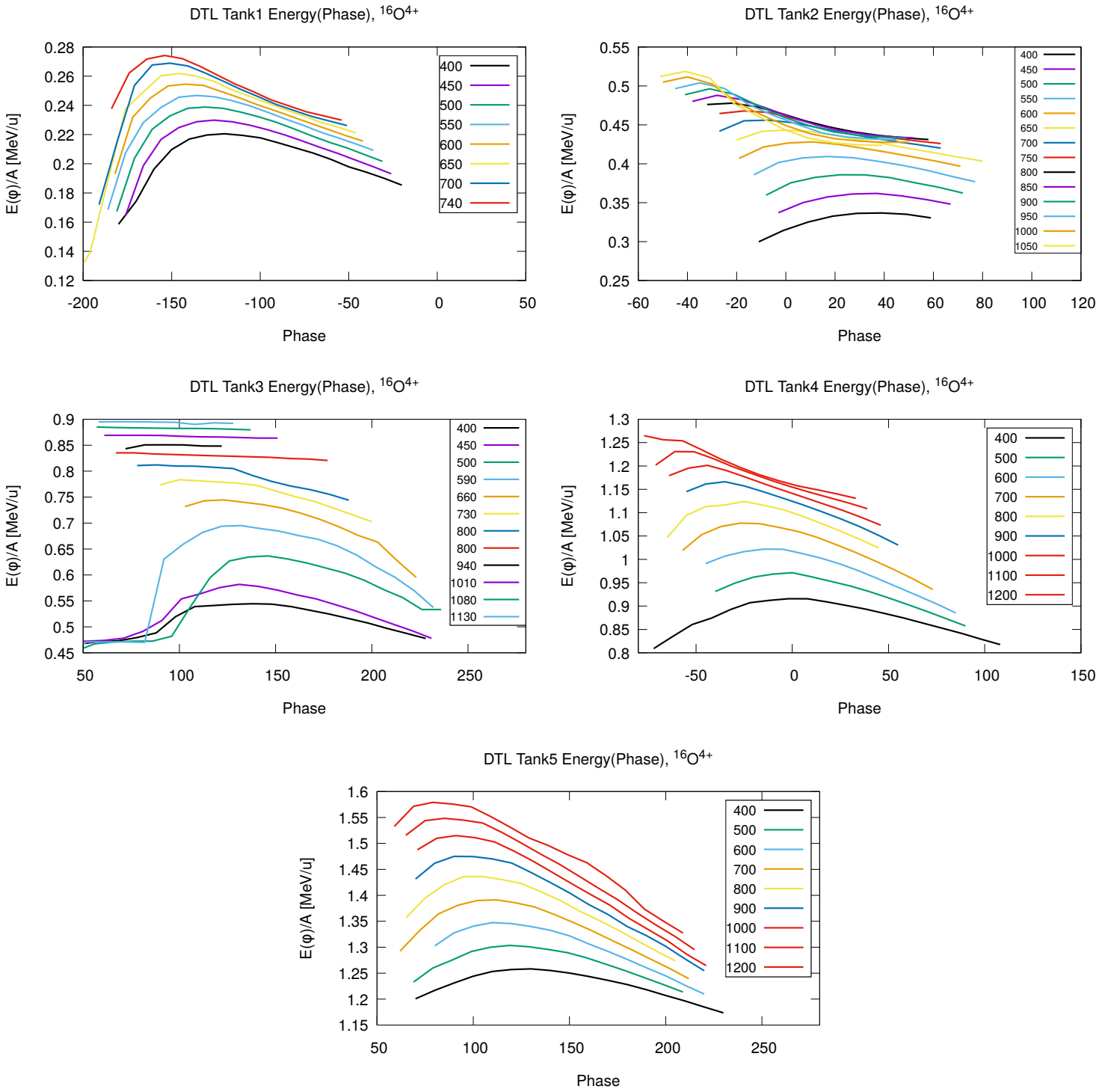

Figure 3: Energy-Phase lines for the ISAC-DTL, as measured with $^{16}O^{4+}$. Amplitude settings, as set by operators via EPICS, are shown in the legend for each plot. Each line shows the linac output for constant amplitude, implying constant on-axis electric field.

3 Opera-2D Longitudinal Electric Field Model

In [3], Baartman develops the F-matrix formalism for an axially symmetric, time varying electric field, as found in many linacs, including the DTL. While the assumption of full axial symmetry is not perfectly true, owing to the presence of a small dipole component arising from the IH structure's stems, the tank design aims to minimize this, and for the ISAC-DTL it is negligible [17]. To produce the TRANSOPTR model, the dimensions of the as-built drift tubes were kindly provided by R. Laxdal and B. Waraich and were used to cross-reference technical drawings obtained from the TRIUMF Design Office. As the acceleration through the linac depends entirely on the field $\mathcal{E}(s)$, incorrect dimensions would likely produce an output energy spectrum which would disagree with observations.

3.1 Opera-2D $\mathcal{E}(s)$ Model and Dimensions

The electromagnetic code Opera-2D was used to generate a model of the drift tubes for each resonator in the DTL using the provided dimensions, following a geometric model shown in Figure 4. The dimensions for the bunchers were obtained from [18], which records the design dimensions from the team at INR-RAS in Moscow. All dimensions and corresponding drawings are listed in Tables 2, 3 and 4.

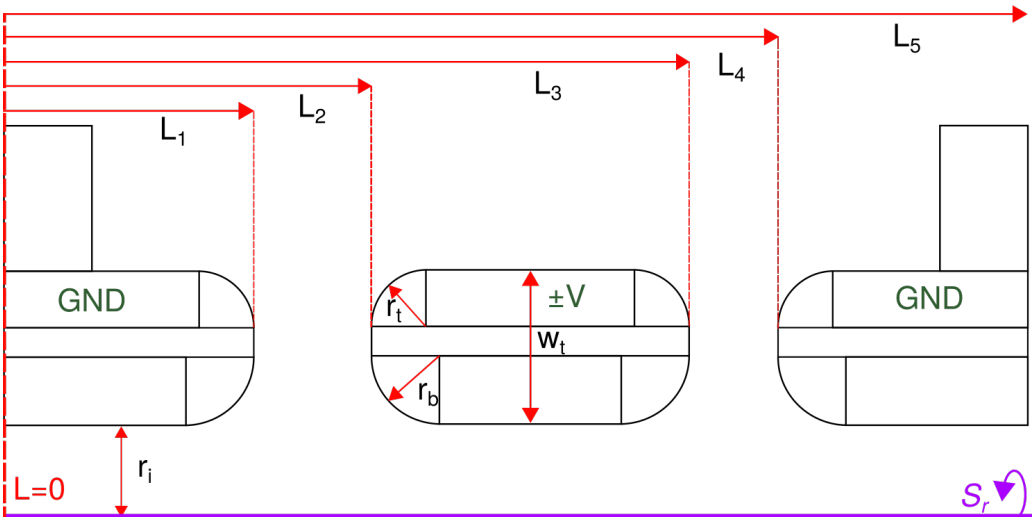

Figure 4: Geometric representation of the Opera-2D model used for the axially symmetric IH-structure geometry, showing a single drift tube as an example, between two outer tubes connected to the cavity wall. The axis of radial symmetry is shown in purple, labelled S_r. The outer tubes are grounded (GND) while the inner tube(s) alternate between a constant value of $\pm V$. Tube dimensions, including rounded edge radii and tube lengths have been extracted from design drawings or specified reference.

tube start [in]	tube end [in]	V [kV]
0.000	1.6927	0.0
2.188	2.6788	-1.0
3.209	3.7030	1.0
4.260	4.7672	-1.0
5.341	5.8721	1.0
6.447	7.0165	-1.0
7.596	8.2034	1.0
8.763	9.4284	-1.0
9.960	10.6693	1.0
11.200	12.8923	0.0

tube start [in]	tube end [in]	V [kV]
0.0000	1.5330	0.0
2.0300	2.8170	-1.0
3.3390	4.1320	1.0
4.6910	5.4840	-1.0
6.0780	6.8790	1.0
7.5000	8.3150	-1.0
8.9560	9.7910	1.0
10.4480	11.3090	-1.0
11.9740	12.8710	1.0
13.5310	14.4770	-1.0
15.1180	16.1240	1.0
16.7370	17.8060	-1.0
18.3910	19.5030	1.0
20.0960	21.6850	0.0

Table 2: Physical drift tube dimensions for (**Left**) DTL Tank-1, extracted from drawing `IRF0571D.dwg` (Fig. 5) and (**Right**) DTL Tank-2, from drawing `IRF1102D.dwg` (Fig. 6), obtained from the TRIUMF Design Office.

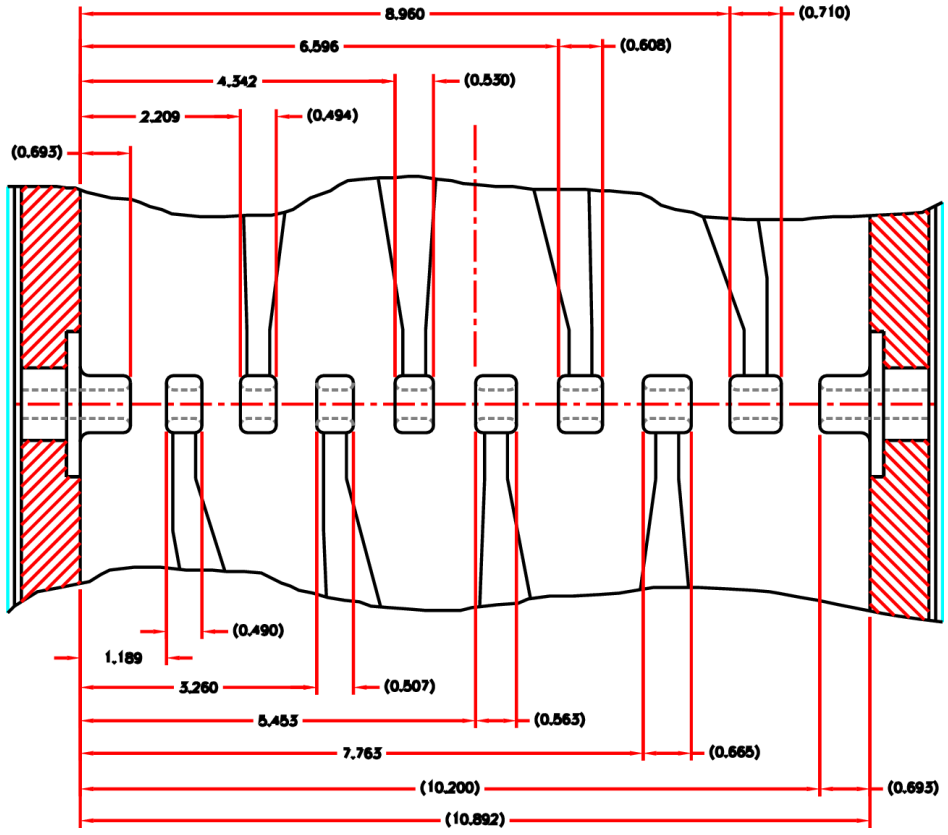

Figure 5: **Top:** `IRF0571D.dwg`, showing the interdigital structure within DTL Tank-1. Extracted tube lengths are listed in Table 2.

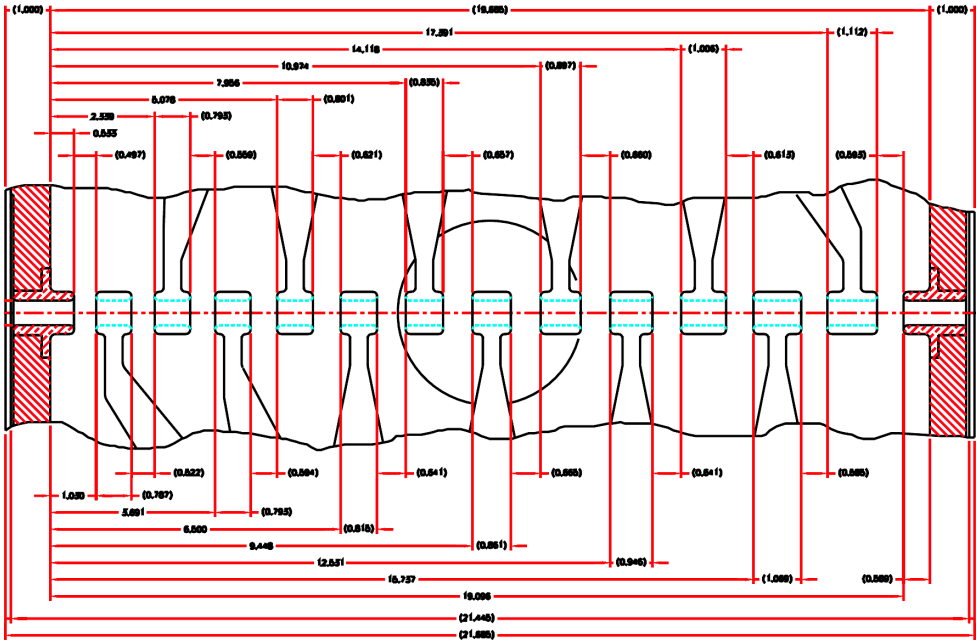

Figure 6: `IRF1102D.dwg`, showing the interdigital structure within DTL Tank-2. Extracted tube lengths are listed in Table 2.

tube start [in]	tube end [in]	v [kv]
0.0000	1.5230	0.0
2.1900	3.2850	-1.0
3.9620	5.0630	1.0
5.7910	6.8750	-1.0
7.6630	8.7350	1.0
9.5650	10.6380	-1.0
11.5040	12.5840	1.0
13.4810	14.5760	-1.0
15.4930	16.6160	1.0
17.5380	18.6980	-1.0
19.6220	20.8250	1.0
21.7410	23.0020	-1.0
23.8910	25.2240	1.0
26.0730	27.4830	-1.0
28.2950	29.7540	1.0
30.5750	32.1950	0.0

tube start [in]	tube end [in]	V [kV]
0.0000	1.4170	0.0
2.3450	3.7250	-1.0
4.6650	6.0490	1.0
7.0410	8.4060	-1.0
9.4570	10.8100	1.0
11.9020	13.2540	-1.0
14.3180	15.7460	1.0
16.8900	18.2780	-1.0
19.4340	20.8560	1.0
22.0080	23.4810	-1.0
24.6100	26.1450	1.0
27.2470	28.8510	-1.0
29.9130	31.5790	1.0
32.6280	34.3290	-1.0
35.3870	37.3130	0.0

Table 3: Physical drift tube dimensions for (**Left**) DTL Tank-3, extracted from drawing `IRF1183D.dwg` (Fig. 7) and (**Right**) DTL Tank-4, from drawing `IRF1243D.dwg` (Fig. 8, top), obtained from the TRIUMF Design Office.

tube start [in]	tube end [in]	V [kV]
0.0000	1.4490	0.0
2.6850	4.2220	-1.0
5.4700	7.0240	1.0
8.2970	9.8600	-1.0
11.1640	12.7440	1.0
14.0580	15.6660	-1.0
16.9860	18.6280	1.0
19.9860	21.6340	-1.0
22.9340	24.6790	1.0
25.9510	27.7650	-1.0
28.9960	30.8960	1.0
32.0610	34.0360	-1.0
35.1820	37.1940	1.0
38.3490	40.4630	0.0

Table 4: Physical dimensions extracted from drawing `IRF1302D.dwg` (Fig. 8, bottom) for ISAC-DTL Tank-5, 106.08 MHz.

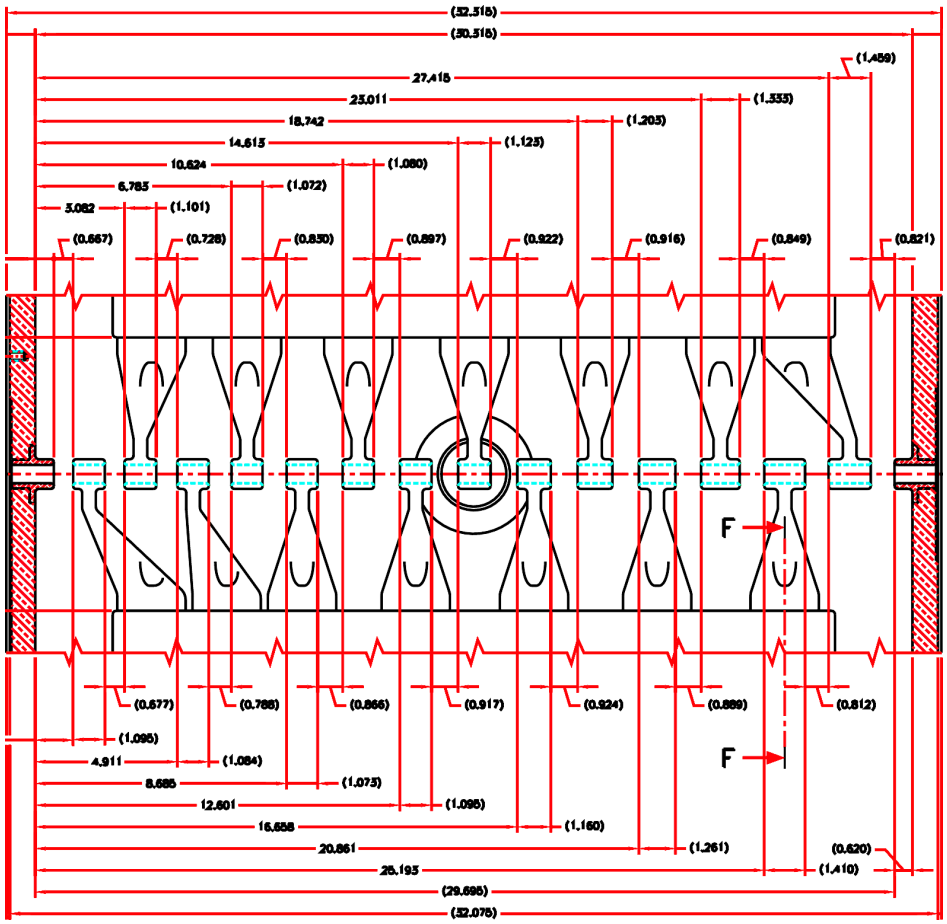

Figure 7: **Top:** `IRF1183D.dwg`, showing the interdigital structure within DTL Tank-3. Extracted tube lengths are listed in Table 3.

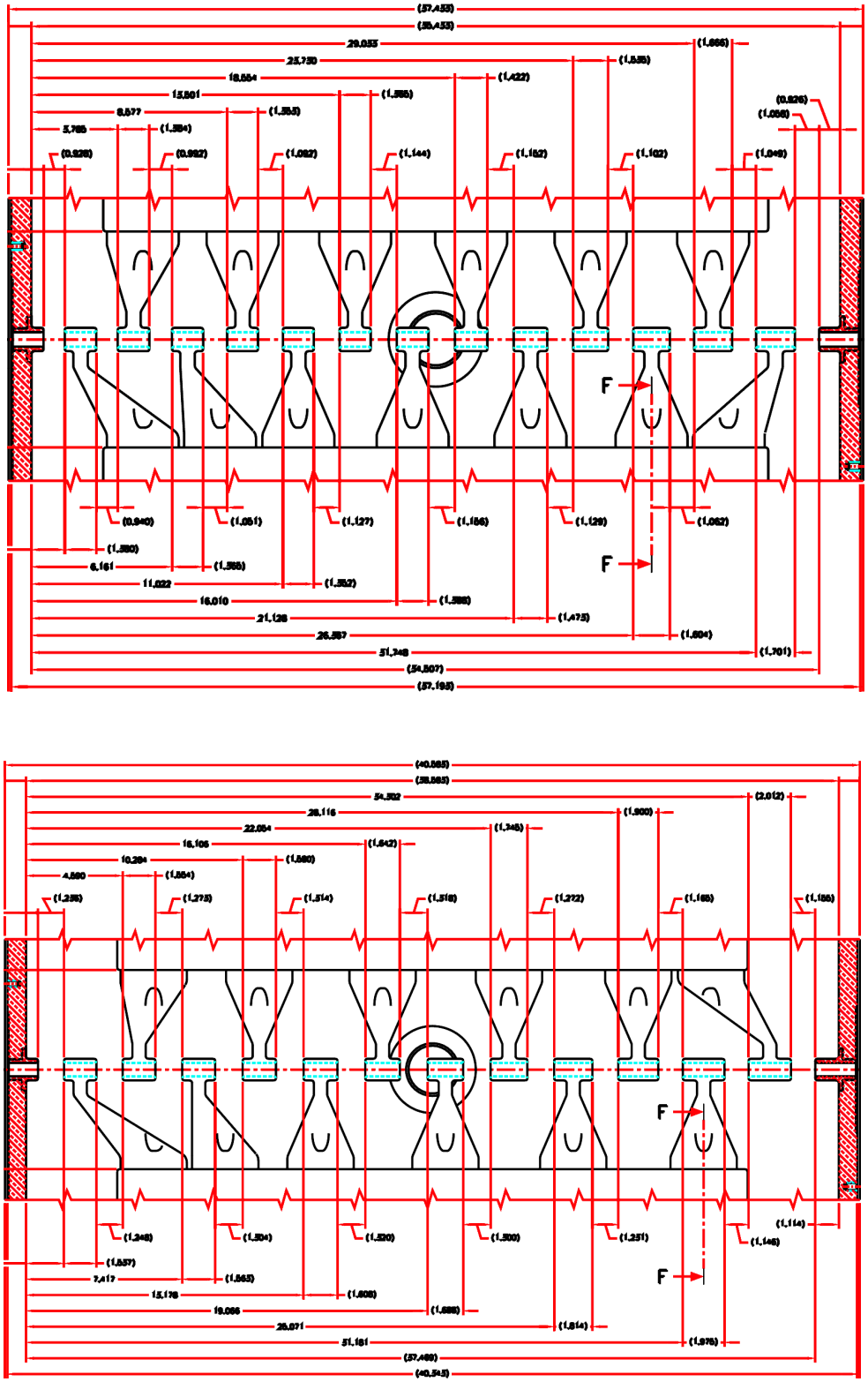

Figure 8: **Top:** `IRF1243D.dwg`, showing the interdigital structure within DTL Tank-4. **Bottom:** `IRF1303D.dwg`, DTL Tank-5. Extracted tube lengths for both tanks are listed in Table 3. **Drawings not to scale with respect to each other.**

Additional simulation parameters for the DTL tanks, corresponding to those shown in Figure 4 are shown in Table 5. For the bunchers, the extracted dimensions are shown in Table 6, with the tube-specific parameters listed in Table 7. The technical drawing `IRF0965D.dwg` is shown in Figure 9, obtained from INR-RAS, representing the thre-gap DTL bunchers.[1]. Note that the tube dimensions shown in the figure are a placeholder, with the final as-built dimensions listed in ref. [18].

Cavity	No. Tubes	W_t[in]	$r_b = r_t$ [in]	r_i [in]	s_{end} [in]
IH Tank-1	8	0.1970	0.0938	0.2755	12.8923
IH Tank-2	12	0.2953	0.0985	0.19685	21.6850
IH Tank-3	14	0.1970	0.0938	0.3150	32.1950
IH Tank-4	13	0.1970	0.0938	0.3150	37.3130
IH Tank-5	12	0.1970	0.0938	0.3150	40.4630

Table 5: Extracted tube dimensions for each tank, showing the cavity name, number of drift tubes (excluding grounded end tubes), the tube thickness W_t, rounded edge radii, which is equal for the IH cavities, in addition to the tube inner radius r_i and end coordinate of the field map $\mathcal{E}(s)$. All dimensions are in inches as presented on the technical drawings.

tube start [in]	tube end [in]	V [kV]
0.0000	0.9853	0.0
1.2302	2.1295	-1.0
2.6729	3.5756	1.0
3.8186	4.8226	0.0

tube start [in]	tube end [in]	V [kV]
0.0000	1.5481	0.0
1.7631	2.9229	-1.0
3.4229	4.0835	1.0
4.2985	5.8466	0.0

tube start [in]	tube end [in]	V [kV]
0.0000	1.6935	0.0
2.0033	3.31355	-1.0
3.8520	4.63720	1.0
4.9470	6.6405	0.0

Table 6: Physical drift tube dimensions for (**Top-Left**) DTL Buncher-1, (**Top-Right**) DTL Buncher-2 and (**Bottom**) DTL Buncher-3, all obtained from [18].

[1] Note the transliteration errors from cyrillic to latin characters in Figure 9

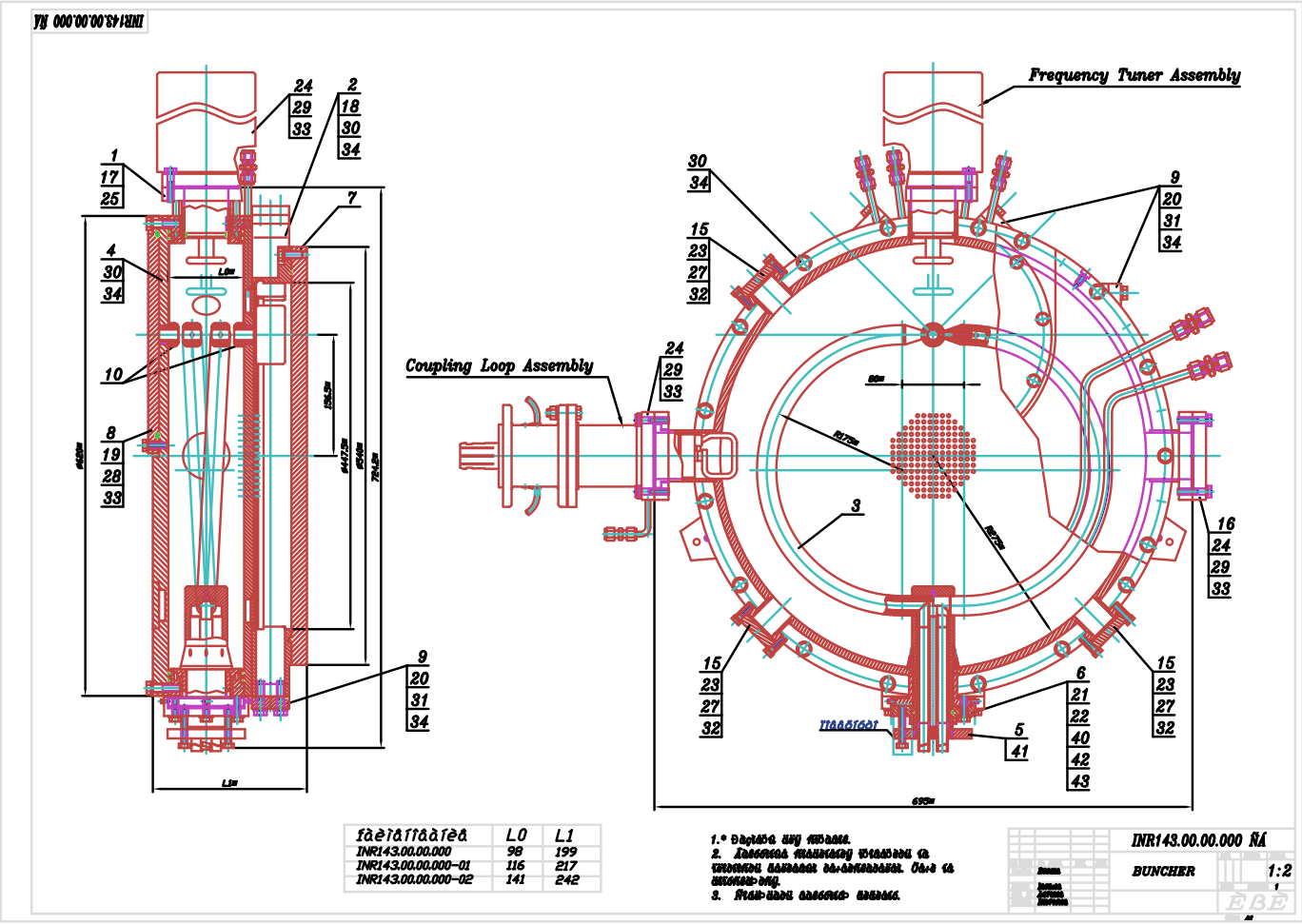

Figure 9: Digitized design drawing for the 3-gap spiral DTL bunchers, originally from INR-RAS, used for `Opera2D` field map generation. Note the transliteration errors representing original cyrillic characters. Dimensions as shown in the drawing are in millimeters, and are valid. Obtained from the TRIUMF Design Office. Note, the technical drawing is identical to that for the MEBT bunch rotator, shown in [9].

Cavity	No. Tubes	W_t[in]	r_b [in]	r_t [in]	r_i [in]	s_{end} [in]
Buncher-1	2	0.3150	0.0987	0.1392	0.4918	4.8226
Buncher-2	2	0.3150	0.0987	0.1392	0.4918	5.8466
Buncher-3	2	0.3150	0.0987	0.1392	0.4918	6.6405

Table 7: Extracted tube dimensions for each buncher, showing the cavity name, number of drift tubes (excluding grounded end tubes), the tube thickness W_t, rounded edge radii r_t and r_b, in addition to the tube inner radius r_i and end coordinate of the field map $\mathcal{E}(s)$. All dimensions are in inches as presented on the technical drawings.

3.2 `Opera-2D` On-Axis Electric Fields

The model for each tank and buncher was processed in `Opera-2D` allowing for the generation of an on-axis electric field distribution $\mathcal{E}(s)$ for each RF component of the DTL, enabling the use of `TRANSOPTR` subroutine `linac` for each cavity, with outputs listed in Table 8.

It is noted that unlike published bead pull measurements (e.g. Fig. 3 in [19]), the `Opera-2D` output field distributions possess varying peak heights along the length s of the structures and that in this implementation, no attempt has been made to manipulate the tube voltages to flatten the peak height distribution. This is noted as a possible model tuning strategy, though will not be further explored in this report.

RF Cavity	Figure
IH Tank-1	Figure 10, t.
Buncher-1	Figure 12, t.
IH Tank-2	Figure 10, b.
Buncher-2	Figure 12, m.
IH Tank-3	Figure 11, t.
Buncher-3	Figure 12, b.
IH Tank-4	Figure 11, m.
IH Tank-5	Figure 11, b.

Table 8: List of figures showing the `Opera-2D` computed fields associated with each RF cavity in the ISAC DTL. Figure placement specified as top (t), middle (m) or bottom (b).

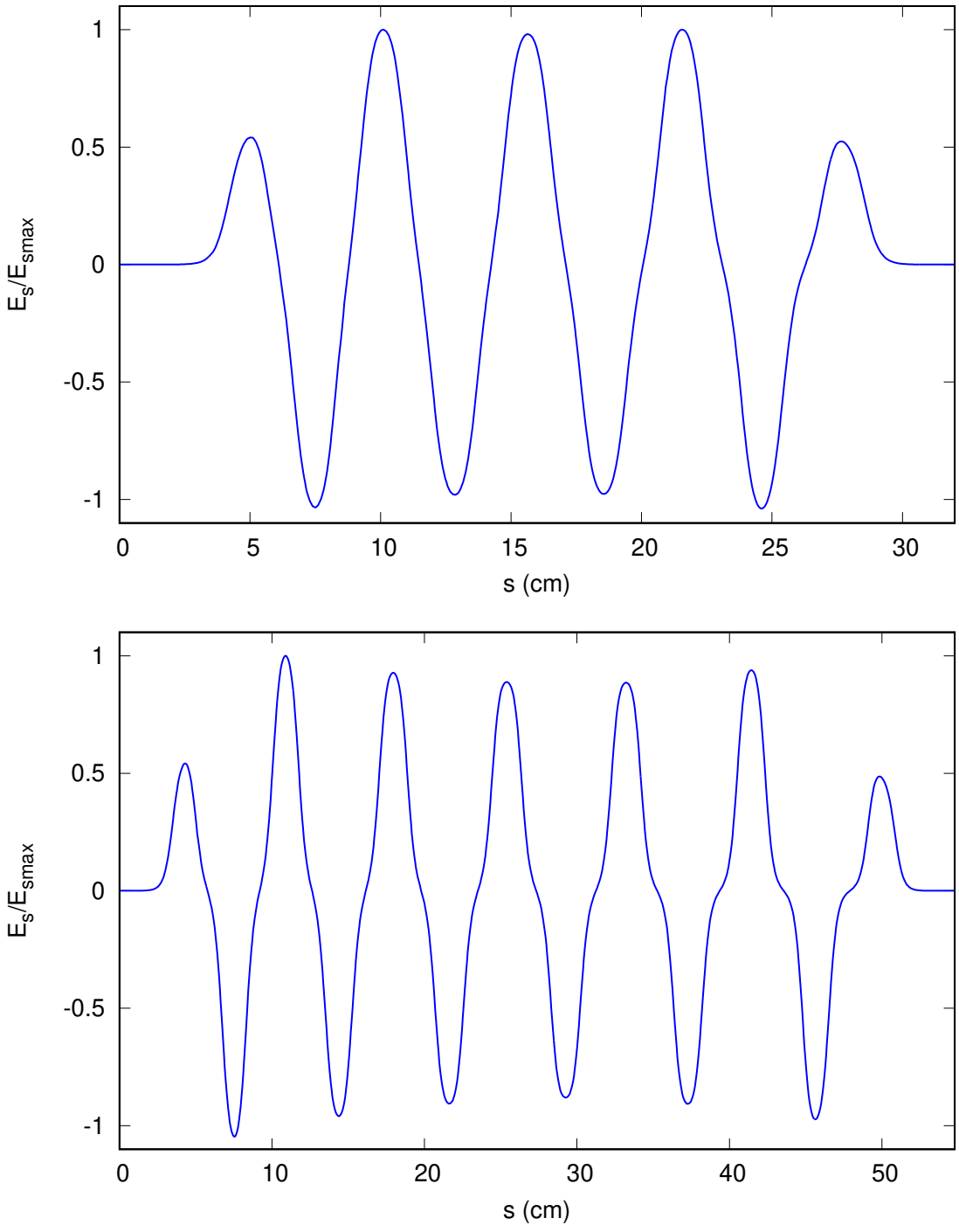

Figure 10: Normalized longitudinal electric field $\mathcal{E}(s)$ for the ISAC Drift Tube Linac, showing (**Top**) Tank-1 and Tank-2 (**Bottom**)

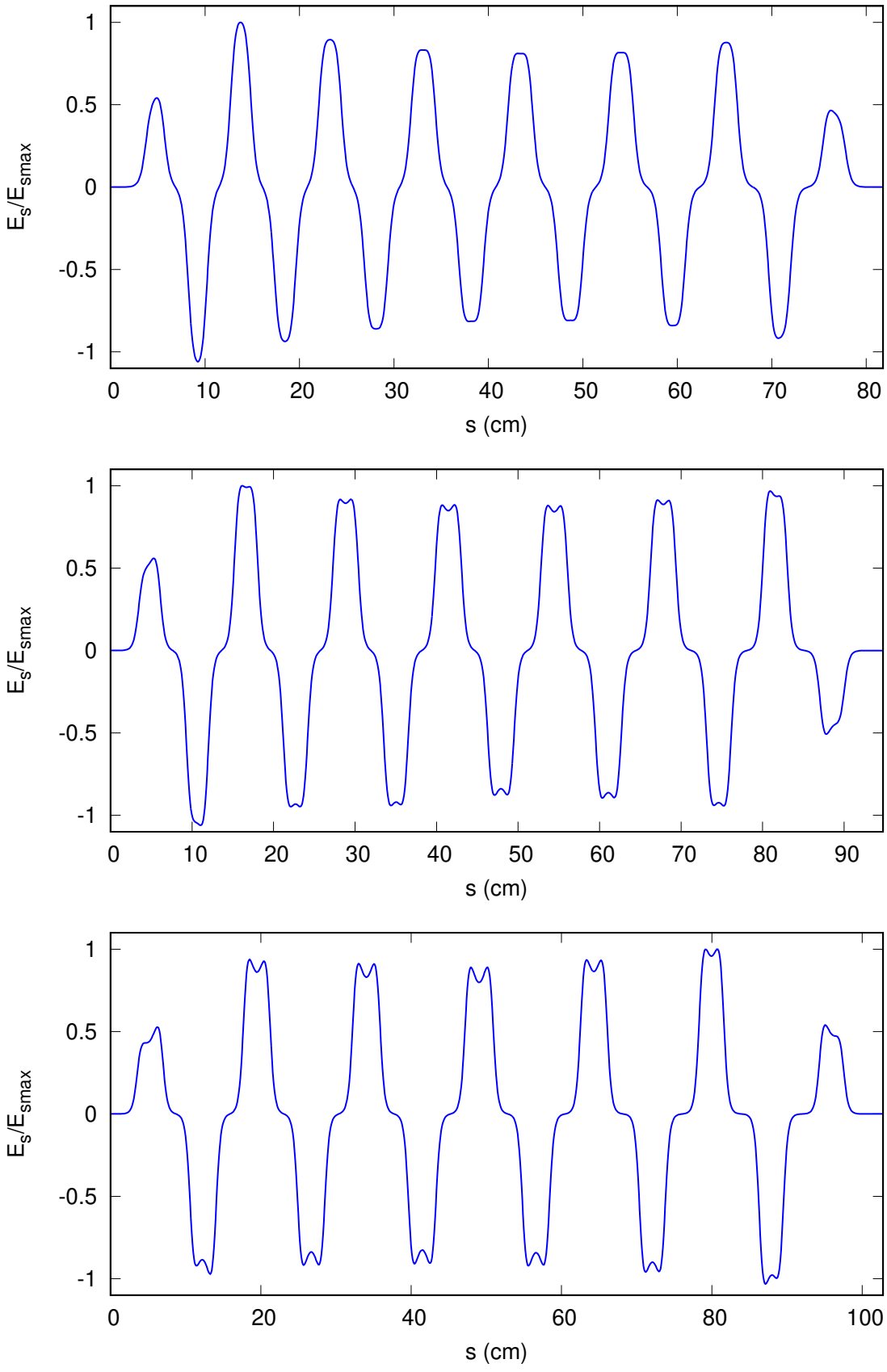

Figure 11: Normalized longitudinal electric field $\mathcal{E}(s)$ for the ISAC Drift Tube Linac, showing Tank-3 (**Top**), Tank-4 (**Middle**) and Tank-5 (**Bottom**).

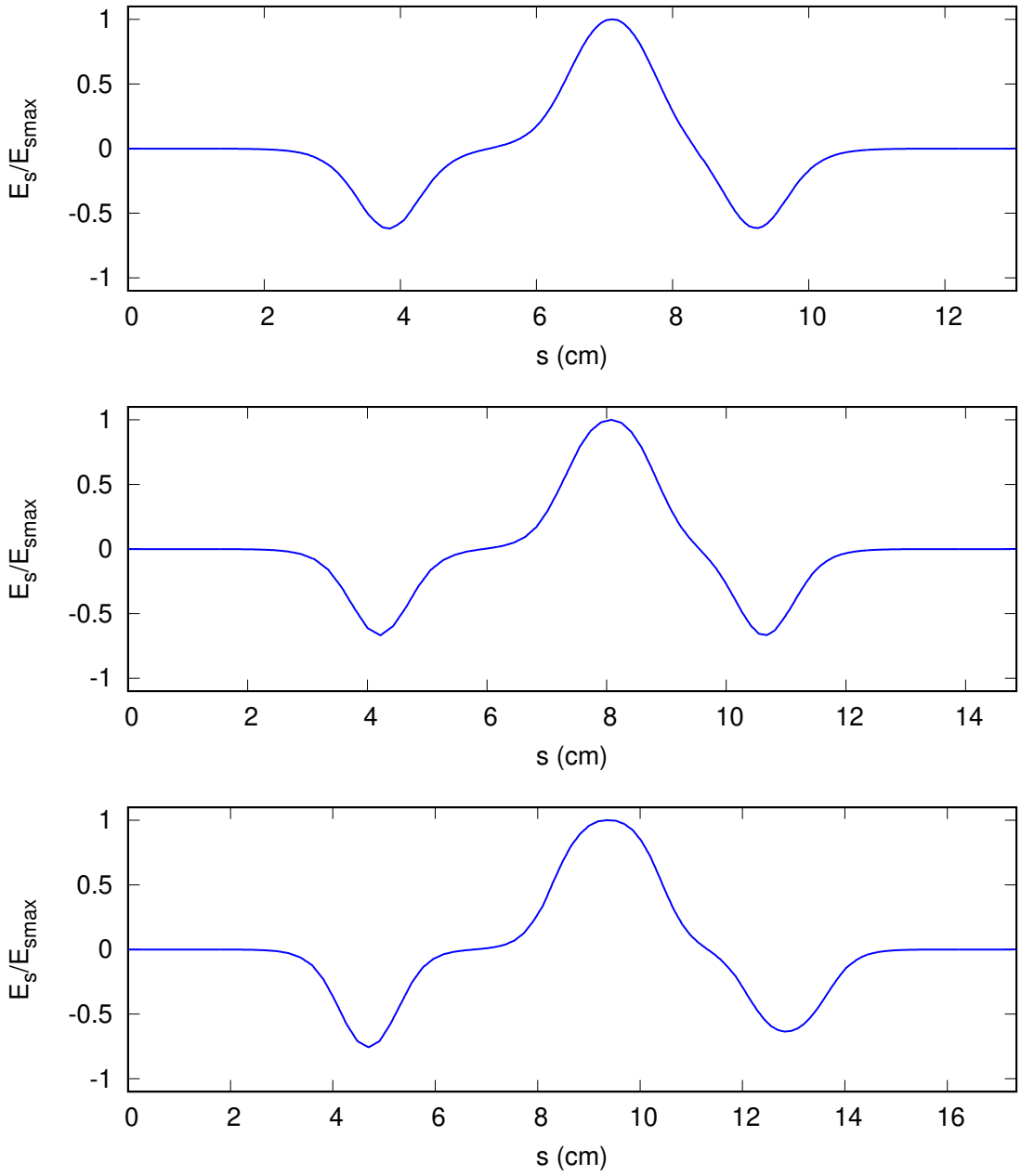

Figure 12: Normalized longitudinal electric field $\mathcal{E}(s)$ for the ISAC Drift Tube Linac, showing Buncher-1 (**Top**), Buncher-2 (Middle) and Buncher-3 (**Bottom**).

4 /acc-database TRANSOPTR Implementation

The model for the linac uses technical drawing IRF1002D.dwg, shown in Figure 1, for tank, buncher and quad positioning along the optical axis s. The field maps from Section 3 are centered at the geometric midpoint of each tank or buncher, referenced to the outer tank surfaces. The sequence dtl_db0.xml in the /acc database has been defined from the above drawing and the sequence layout is shown in Table 9.

sequence dtl_db0			
Start IRF1002D.dwg (x,y)		End IRF1002D.dwg (x,y)	
(51.1528",0.0")		(279.2737",0.0")	
Layout Drawing		Figure 1	
Element Name	Element Type	Position s[mm]	Length L[mm]
start sequence	marker	0.000	0.000
ISAC1:DTL1	linac	163.73	327.50
DTL:Q1	MQuad	382.55	58.000
DTL:Q2	MQuad	512.54	87.000
DTL:Q3	MQuad	609.54	58.000
twiss-x/y	fortline	642.52	N/A
ISAC1:BUNCH1	linac	757.23	130.5
ISAC1:DTL2	linac	1144.87	547.80
DTL:Q4	MQuad	1473.15	58.000
DTL:Q5	MQuad	1603.13	87.000
DTL:Q6	MQuad	1700.13	58.000
twiss-x/y	fortline	1782.62	N/A
ISAC1:BUNCH2	linac	1856.85	148.5
ISAC1:DTL3	linac	2388.47	817.75
DTL:Q7	MQuad	2851.77	58.000
DTL:Q8	MQuad	2981.75	87.000
DTL:Q9	MQuad	3111.74	58.000
twiss-x/y	fortline	3161.24	N/A
ISAC1:BUNCH3	linac	3247.97	173.50
ISAC1:DTL4	linac	3857.09	947.80
DTL:Q10	MQuad	4385.39	58.000
DTL:Q11	MQuad	4515.37	87.000
DTL:Q12	MQuad	4645.36	58.000
twiss-x/y	fortline	4766.51	N/A
ISAC1:DTL5	linac	5280.39	1027.80
end sequence	marker	5794.27	0.000

Table 9: Sequence dtl_db0: the ISAC Drift Tube Linac with reference start and end coordinates from which elements and their positions along the optical axis, S in millimeters were extracted. Quadrupole effective lengths obtained from [20]. The TRANSOPTR element (subroutine) type, in addition to the element length are also displayed.

The quadrupole triplet effective lengths were set to 5.8cm and 8.7cm for the outer and inner quadrupoles, respectively [20]. A detailed analysis of the BI relationship for the DTL quadrupoles may be found in [15].

5 TRANSOPTR Simulations

An initial comparison was performed with an A/q=6 beam using a starting tune based on parameters obtained from [2] for the initial sigma matrix parameters. Optr was run in mode 5, featuring the addition of global time tracking [14], which allows for a time-of-flight based relative tank phasing. The `/acc` database implementation of the HEBT line [10] was used, along with `dtl_db0.xml` to generate a TRANSOPTR system file representing the entire ISAC-DTL, starting at DTL:FC0 and terminating at the HEBT1 high energy diagnostic station (Prague).

The longitudinal tune of the linac was found by performing a comprehensive mapping of the (V_s, ϕ) configuration space of each tank and buncher. This data was used to find the optimum accelerating tank setpoints producing the design energy profile specified in Table 1, in Section 1. These also allowed for the generation of TRANSOPTR computed energy-phase curves at constant V_s, produced to have a maximum energy identical to each constant amplitude line in the datasets from Section 2. The comparison of the optr scaling factor V_s with the EPICS PV setpoints allows for the extraction of an initial calibration between both, important for on-line use.

5.1 Beam Based TRANSOPTR Amplitude Calibration

The simulation data from the previous section produces a set of energy-phase curves which can serve as an observable prediction to be compared with beam-based measurements, an initial test of model validity. For this, a modified version of `topology` [21], which found the minimum V_i that can produce an output energy $E_i(V_i, \phi)$ corresponding to the peak energy of each beam-acquired dataset.

The phases which are presented are relative, no calibration has yet been established between the master RF clock which is controlled in EPICS and the TRANSOPTR model's phase. In principle, this means the value of the phase will disagree between model and machine, but the relative phase differences between cavities should be the same, taking into account time-of-flight. The specified tolerance between model maximum output energy and beam-based data, for each scan, was $\Delta E/E$ = 10^{-5}. This corresponds to finding the maximum $\mathcal{T}(V_s, \phi_0)$ [22]. For DTL Tank-1, Buncher-1 and Tank-2, this is shown in Figure 13. For Buncher-2, Tank-3 and Buncher-3, it is shown in Figure 14. Tanks 4 and 5 are in Figure 15. The figures show the correspondence established between the EPICS PV's from the beam measurements and the model. Initial conditions are shown in Tables 10 and 11.

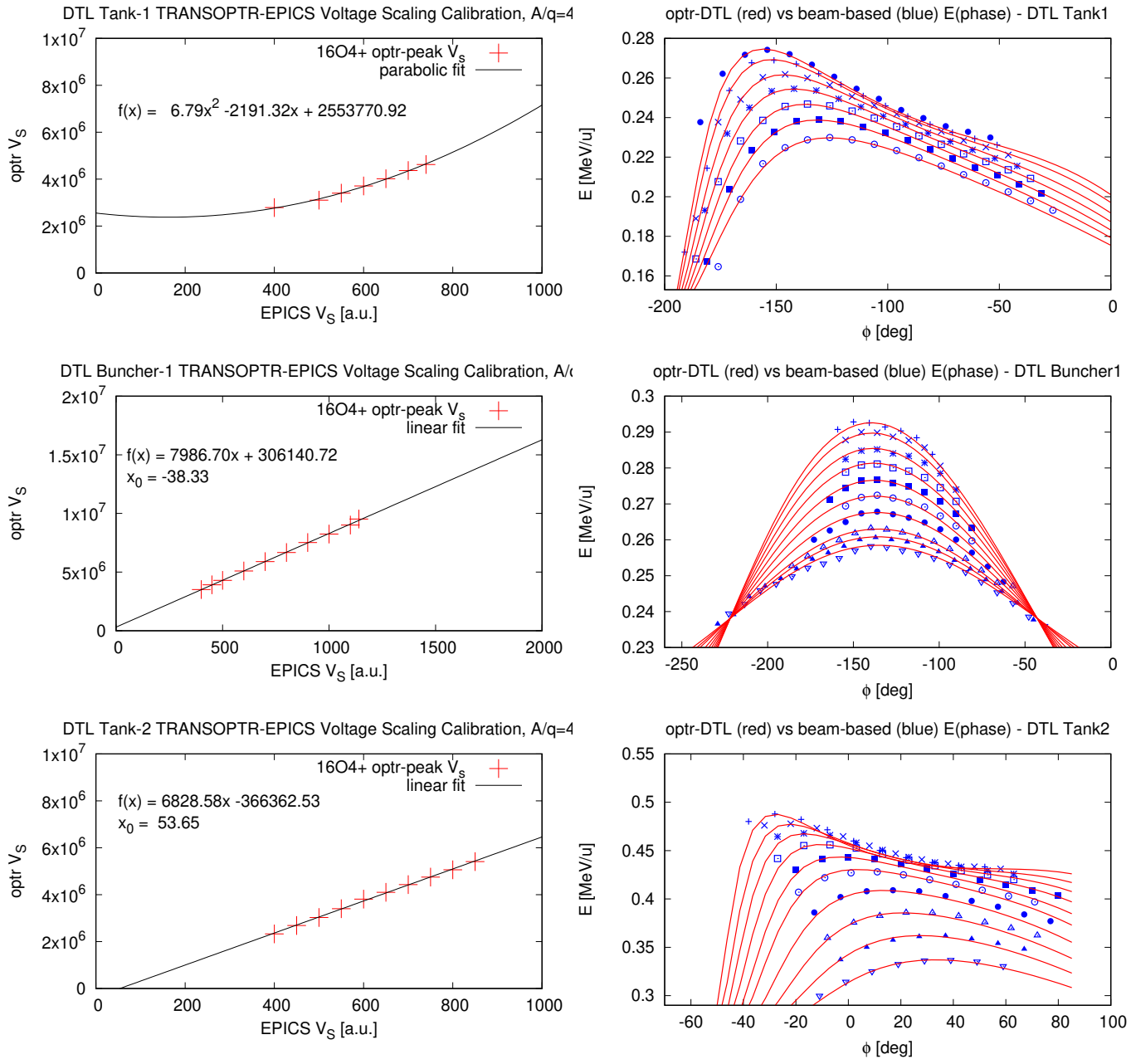

Figure 13: **Top-Left:** Calibration of EPICS voltage scaling factor and TRANSOPTR V_s for DTL Tank-1. **Top-Right:** corresponding TRANSOPTR E(ϕ_0) curves. **Middle:** Corresponding curves for DTL Buncher-1. **Bottom:** Corresponding curves for DTL Tank-2. Based on $^{16}O^{4+}$ data acquired at HEBT1 diagnostic station. Note the phase axes have not been calibrated in this figure.

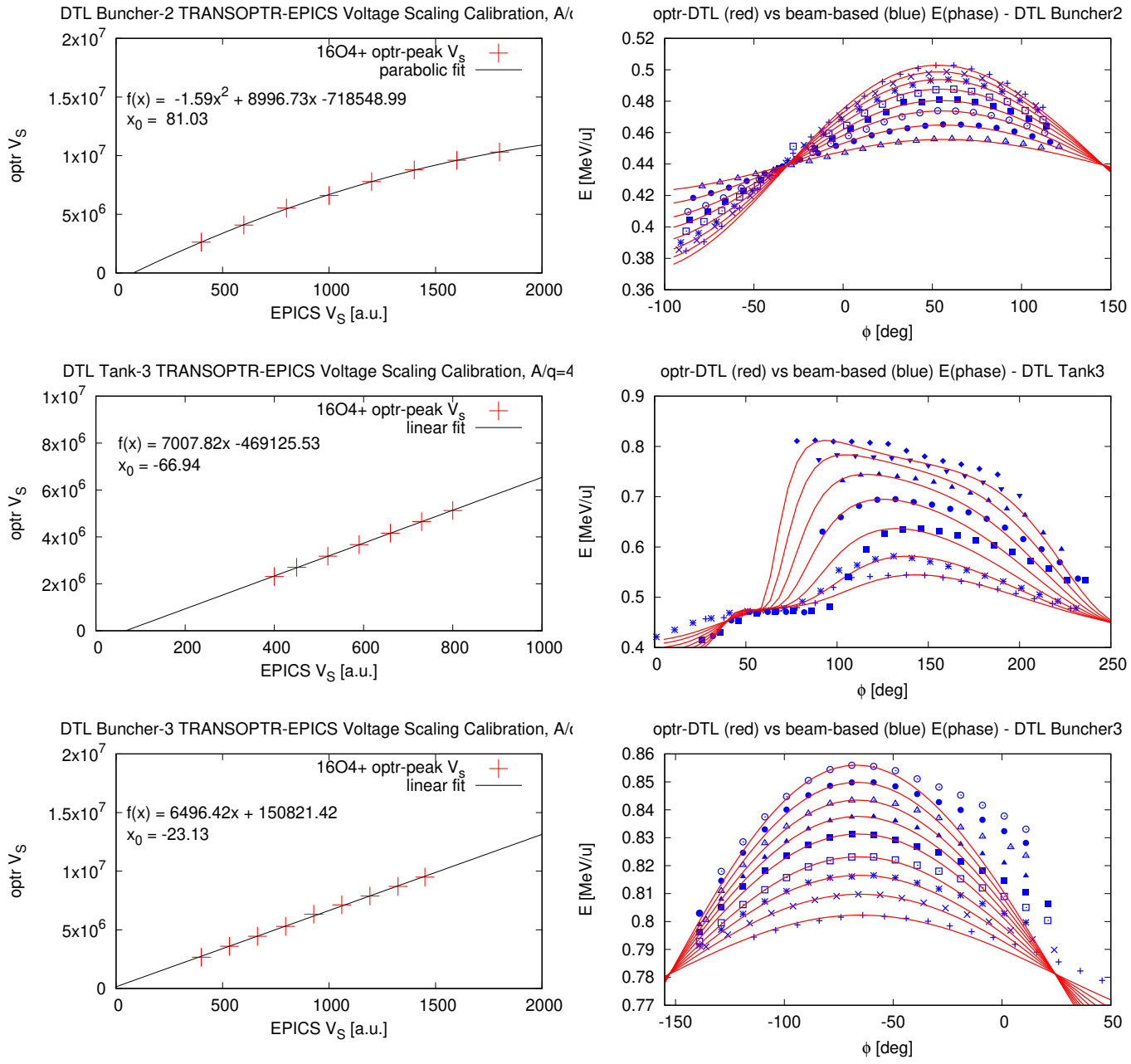

Figure 14: **Top-Left:** Calibration of EPICS voltage scaling factor and TRANSOPTR V_s for DTL Buncher-2. **Top-Right:** corresponding TRANSOPTR E(ϕ_0) curves. **Middle:** Corresponding curves for DTL Tank-3. **Bottom:** Corresponding curves for DTL Buncher-3. Based on $^{16}O^{4+}$ data acquired at HEBT1 diagnostic station. Note the phase axes have not been calibrated in this figure.

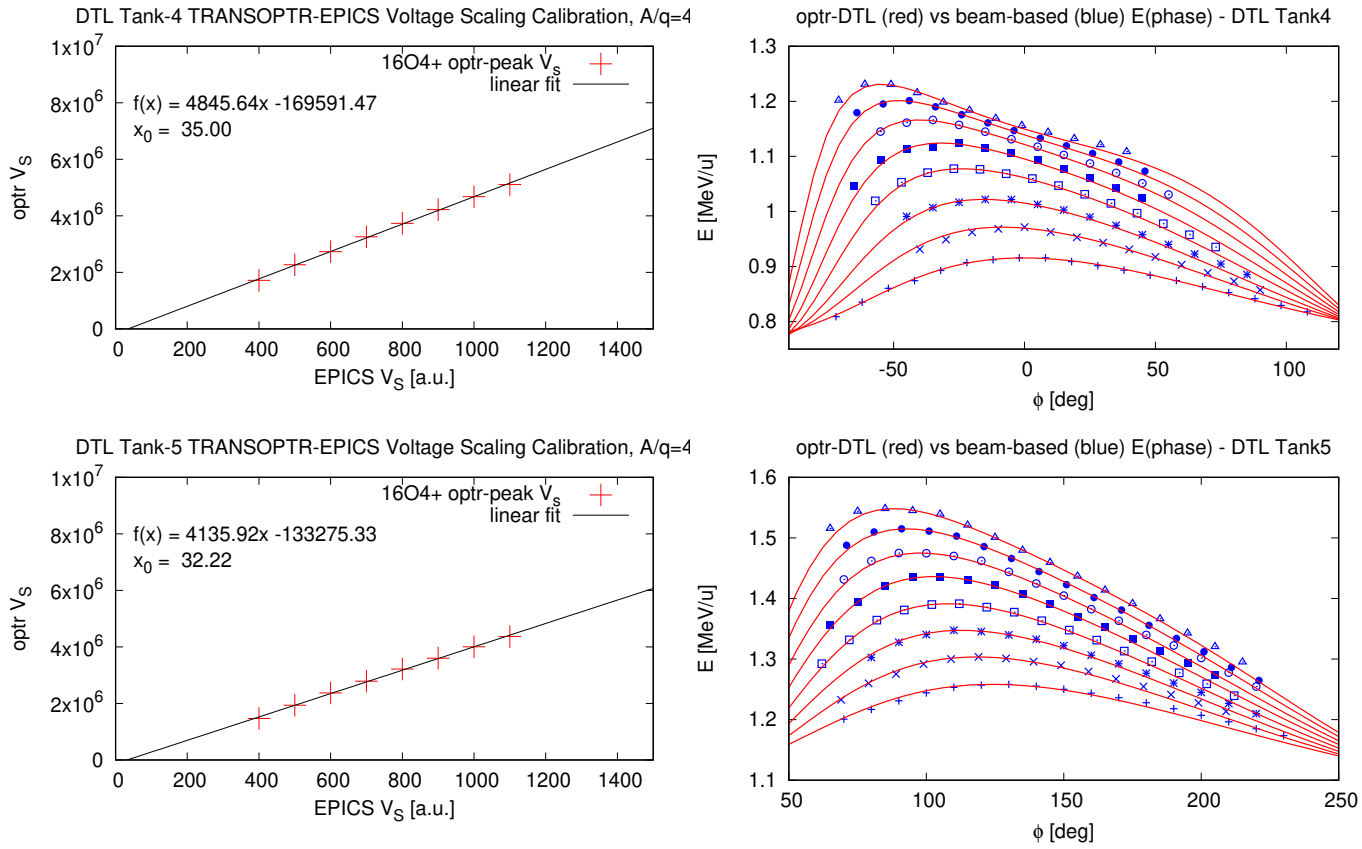

Figure 15: **Top-Left:** Calibration of EPICS voltage scaling factor and TRANSOPTR V_s for DTL Tank-4. **Top-Right:** corresponding TRANSOPTR E(ϕ_0) curves. **Bottom:** Corresponding curves for DTL Tank-5. Based on $^{16}O^{4+}$ data acquired at HEBT1 diagnostic station. Note the phase axes have not been calibrated in this figure.

ϵ_x [μm]	ϵ_y [μm]	ϵ_z [μm]	$r_{xx'}$	$r_{yy'}$	$r_{zz'}$
39.8	34.0	26.7	-0.89	-0.90	-0.62

Table 10: Starting emittances and bunch correlation coefficients between canonical coordinates used for TRANSOPTR-DTL simulations.

E_i [MeV]	m_0 [u]	q [e]	2x-rms [cm]	$2P_x$-rms [mrad]	2y-rms [cm]	$2P_y$-rms [mrad]	2-zrms [cm]	$2P_z$-rms [mrad]
4.59	30.0	5	0.36	23.60	0.34	22.54	0.14	25.17

Table 11: TRANSOPTR DTL injection parameters at start of sequence `dtl_db0.xml`, used for present analysis. The parameters are derived from [2].

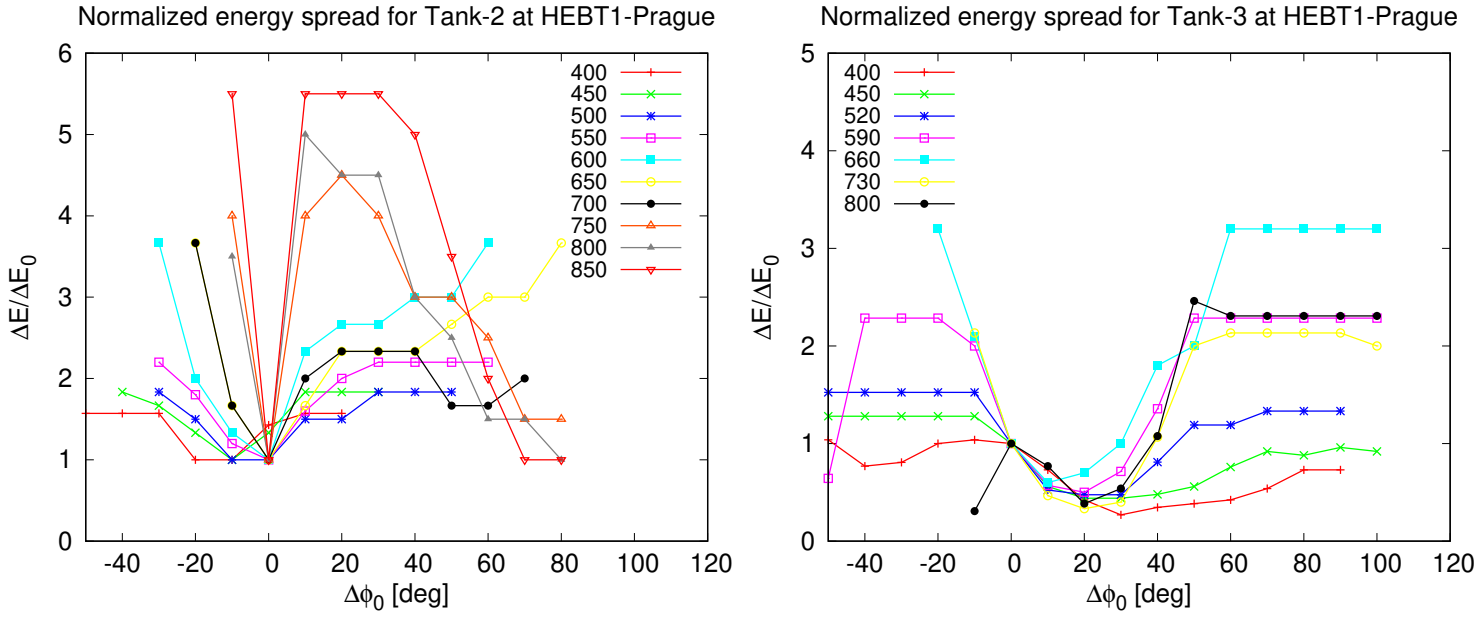

Figure 16: Measured energy spread (FWHM) at HEBT1 HE diagnostic station for $^{16}O^{4+}$ beam, showing normalized, operator estimated energy spread compared to value for maximum output energy at each amplitude, featuring minimized energy spread. The phases are measured with respect to the optimum accelerating phase, showing the rapid growth in energy spread with positive or negative dephasing.

Broadly speaking, the agreement for the cases shown in Figures 13, 14 and 15 can be described as good, with minor disagreements between model and beam. However, for Tank-3 and Buncher-3, in Figure 14, there are notable systematic disagreements in each dataset. In particular, the behavior of the energy-phase curves appears to agree best at maximum accelerating phase for each V_s shown, including Tank/Buncher-3.

There are two separate contributions to this disagreement: measurement uncertainty and model error. With respect to measurement uncertainty, we note that as a result of the predicted growth in energy spread away from the optimum accelerating (V_s, ϕ) means the beam distribution at the HEBT1 diagnostic station will be broad and faint. This makes the identification of an energy centroid difficult on the harp detector. For Tank-2 and Tank-3, the operator estimated energy spread at the Prague-Harp is graphed in Figure 16.

For each tank shown in Fig. 16, we observe the energy spread growing rapidly on either sides of the optimum accelerating phase. Observationally, this means two things. First, as the beam energy spread broadens, the observable distribution on the Prague-Harp monitor likewise broadens and correspondingly drops in intensity, making the observation more difficult.

Second, the HEBT1 diagnostic station has not been designed to allow for a full energy spread measurement at any phase. Consequently, as the energy spread grows, the longitudinal energy distribution exceeds the energy range of the beam monitor, meaning it is difficult to identify the precise location of the energy distribution centroid. This is done by eye and is therefore susceptible to interpretation, particularly when attempting to measure the centoid of a broad, low intensity distribution.

It is also important to note that this model uses fields $\mathcal{E}(s)$ which have been generated by solution of an electrostatic boundary value problem, in other words not an RF simulation. Summary examination of the fields in Section 3 does show a tendency for the peak heights to vary with respect to each other, moreso than is implied by the bead-pulls shown in the literature. While an improvement certainly stands to be made by generating such distributions in a full time-dependant code such as `CST-MWS`, the static fields in this document appear sufficient to predict the operational envelope of the machine, which always uses IH tanks at maximum accelerating phase.

With regards to Tank-3, Fig. 16 suggests a band of about 60° where $\Delta E/\Delta E_0$ remains near or below unity and the likely measurement error small. Beyond this, the growth in energy spread renders the measurement more uncertain, especially at higher energy. As a testament to this, note that the red curve for EPICS amplitude 400 in Fig. 16 suggests a relatively small energy spread for each of the measured phases. Inspection of Figure 14 (middle) for Tank-3 shows that the lower two amplitude energy-phase lines, which starts with A=400, agree most closely with the model, especially when compared to the higher energies in the set.

For Buncher-3, the disagreement is more interesting, owing to a note that was written during data acquisition, shown in Figure 17, where the effect of DTL Buncher-3 upon the beam's energy spread was sketched. The input distribution (left) exits the buncher with a double-peak feature, shown on the right. The note specifies that the high energy tail, corresponding to the narrower, higher energy distribution, was measured off-peak phase.

This can be appreciated in Figure 14, bottom-right, where for each phase-scan, the measured beam energy is seen to vary less than what `TRANSOPTR` predicted, on the positive side of the optimum accelerating phase. The agreement is much better to the negative side, where such deformation was not seen. Certainly, a component of the disagreement between `TRANSOPTR` and the actual DTL measurement must be due to the difference in $\mathcal{E}(s)$. Nevertheless, it would be hazardous to attempt to fine-tune $\mathcal{E}(s)$ on a beam-based dataset, itself which relies upon a set of challenging energy measurements.

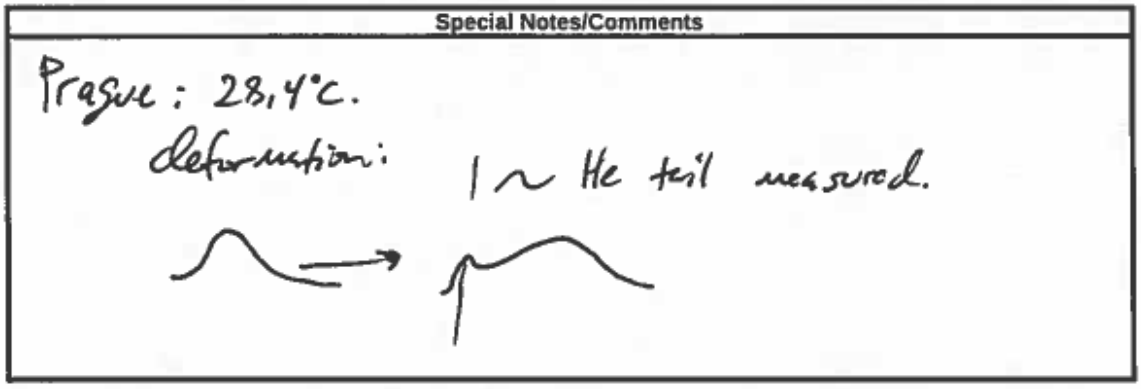

Figure 17: Note taken by author during 2017 data acquisition for DTL Buncher-3. The HEBT1 Magnet (Prague) cooling water temperature is recorded. Observe the recorded energy distribution deformation, where the input beam distribution (left) exits the buncher with a double peak feature, shown on the right.

5.2 Longitudinal Tune and Topological Ramp

The script `topology` was used to perform grid scans of the entire (V_s, ϕ) configuration space of each cavity, in each case spanning the allowable range for both tuning parameters. As in [21], by tracking the output inverse longitudinal momentum P_z at the location of the HEBT1 energy diagnostic, we obtain a signal which is resonant when the energy spread is minimized at a given output energy. Square grid dimensions of 100 or 150 were used to provide sufficient resolution, particularly for the inverted longitudinal momentum, which defines sometimes narrow paths of minimized energy spread through the configuration space.

Output topological scans for the entire DTL are shown in Figures 18, 19 and 20. The inverse z-momentum is shown on the left while the energy is shown on the right, also featuring the extracted path of optimum P_z^{-1}. Each phase-voltage ramp for each cavity is bounded by green triangles, denoting the (lower) injection and (higher) design output energy, from Table 1. Note that the ISAC-DTL RF amplifiers are usually powered on at around A=400, in many cases exceeding the bunching energy, especially in the IH tanks. Observe the relatively narrow band of observable P_z for Tank-3 in Fig. 20, when compared to other accelerating tanks in the machine. To the right of each plot is the output energy for each tank and buncher, also versus phase and voltage.

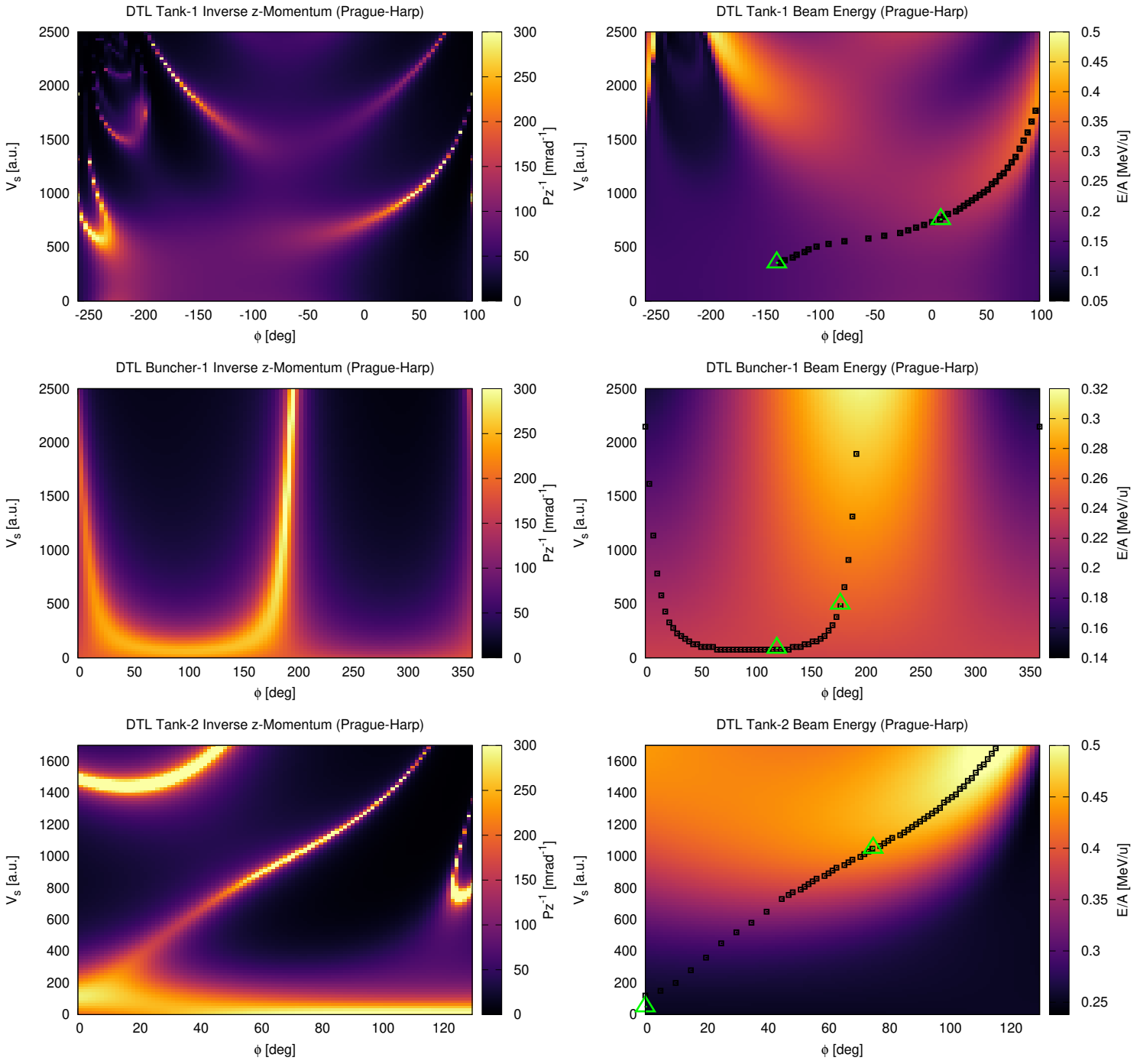

Figure 18: TRANSOPTR grid scans for (**Left**) P_z^{-1} and (**Right**) energy, for (**Top**) DTL Tank-1, (**Middle**) DTL Buncher-1 and (**Bottom**) DTL Tank-2. A/q=30/5 beam used at 0.153 MeV/u initial injection, with preceding cavities set to design energies as per Table 1. The energy ramp with minimized P_z^{-1} is shown as black dots, bounded by green triangles, which denote the configuration space location of the design injection and output energy for each tank and buncher.

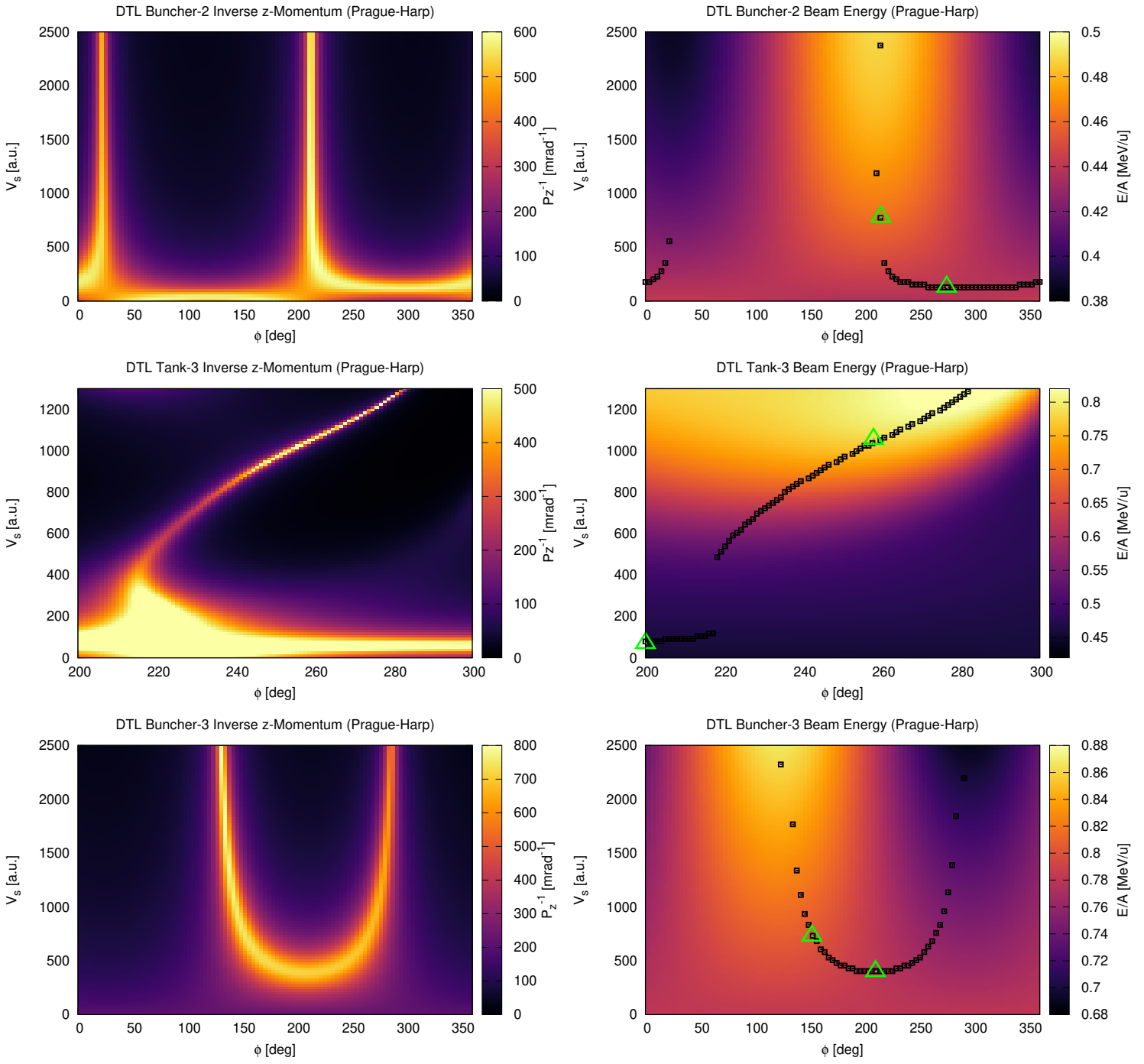

Figure 19: `TRANSOPTR` grid scans for (**Left**) P_z^{-1} and (**Right**) energy, for (**Top**) DTL Buncher-2, (**Middle**) Tank-3 and (**Bottom**) DTL Buncher-3. A/q=30/5 beam used at 0.153 MeV/u initial injection, with preceding cavities set to design energies as per Table 1. The energy ramp with minimized P_z is shown as black dots, bounded by green triangles, which denote the configuration space location of the design injection and output energy for each tank and buncher.

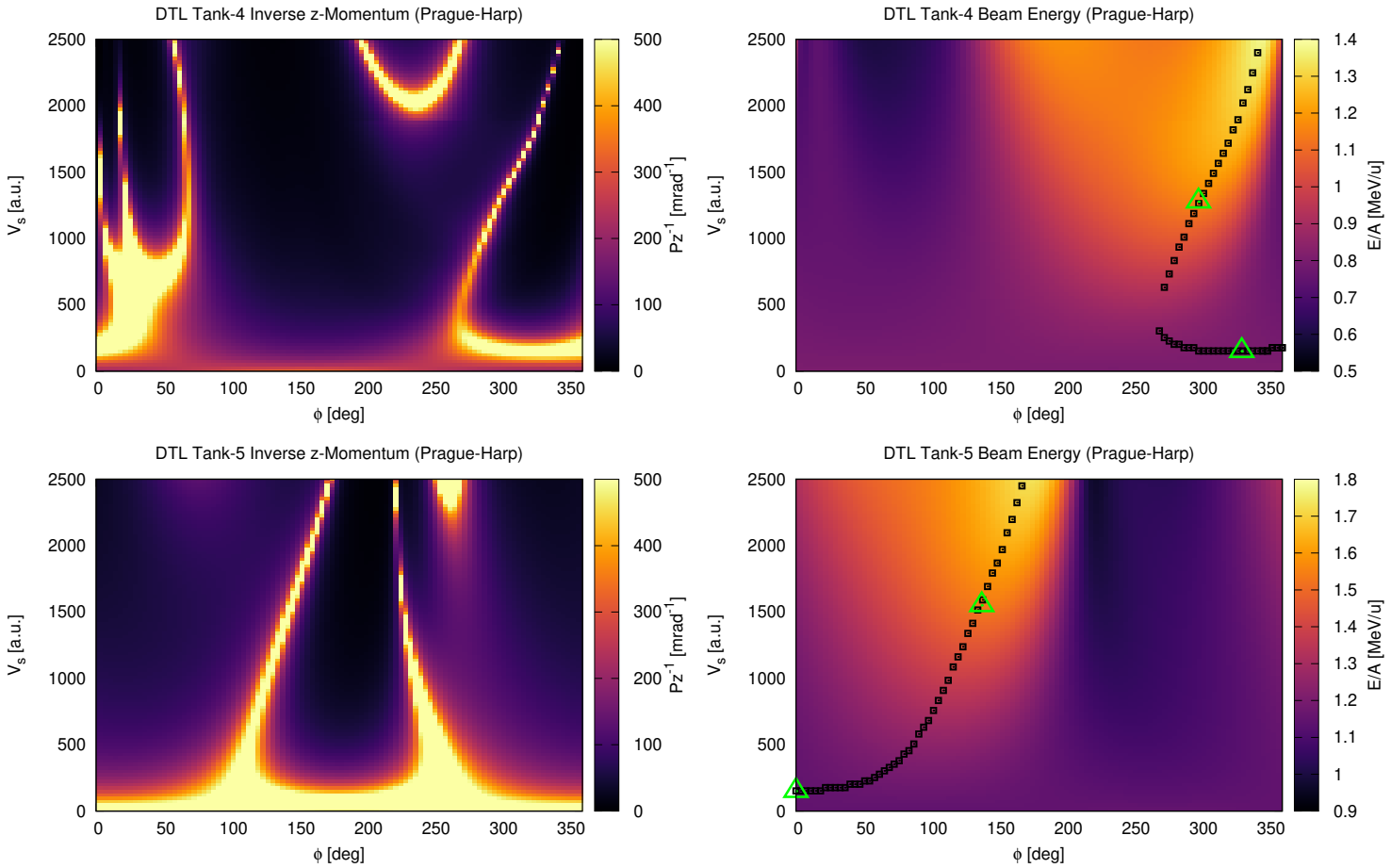

Figure 20: TRANSOPTR grid scans for (**Left**) P_z^{-1} and (**Right**) energy, for (**Top**) DTL Tank-4 and (**Bottom**) DTL Tank-5. A/q=30/5 beam used at 0.153 MeV/u initial injection, with preceding cavities set to design energies as per Table 1. The energy ramp with minimized P_z is shown as black dots, bounded by green triangles, which denote the configuration space location of the design injection and output energy for each tank.

The data shows how TRANSOPTR can be used to explore the longitudinal tune of a variable energy linac, in this case with a prescribed design energy for each tank and buncher. Future investigations can also explore these design energies. The resulting energy-phase ramps are shown in Figure 21 for the IH tanks with the EPICS voltage parameter as the x-axis. The bunchers are shown in Fig. 22, showing the the cosecant-like energy ramp [23]. These plots show the longitudinal tune of the machine (purple), for each corresponding tank output energy (red), at a given voltage setting V_s in the control system. The computed longitudinal tune of the DTL, corresponding to the energies of Table 1 with minimized P_z at the position of the HEBT1 high energy diagnostic, is presented in Table 12.

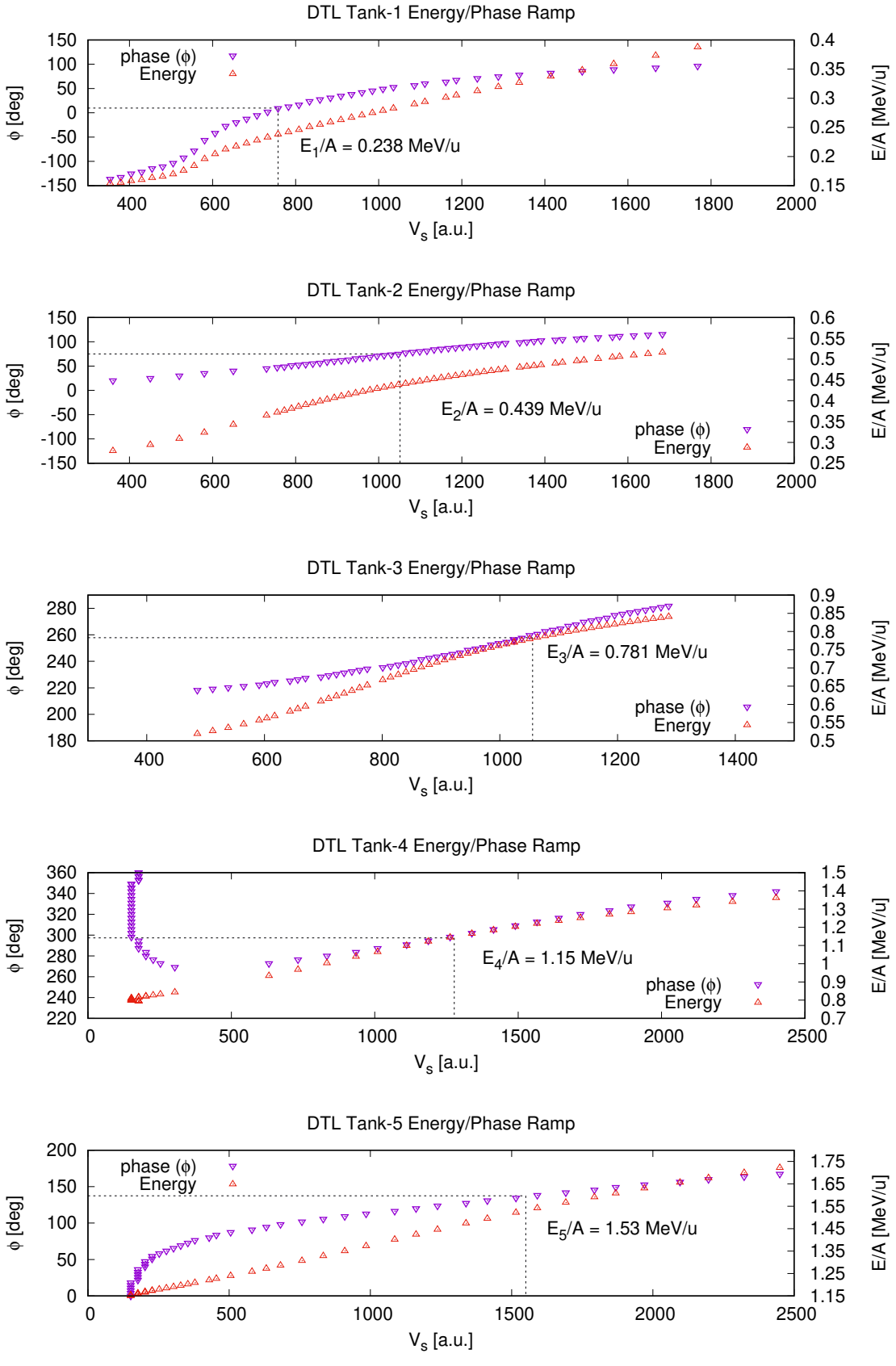

Figure 21: TRANSOPTR Computed DTL Energy-Phase ramps, against EPICS voltage parameter.

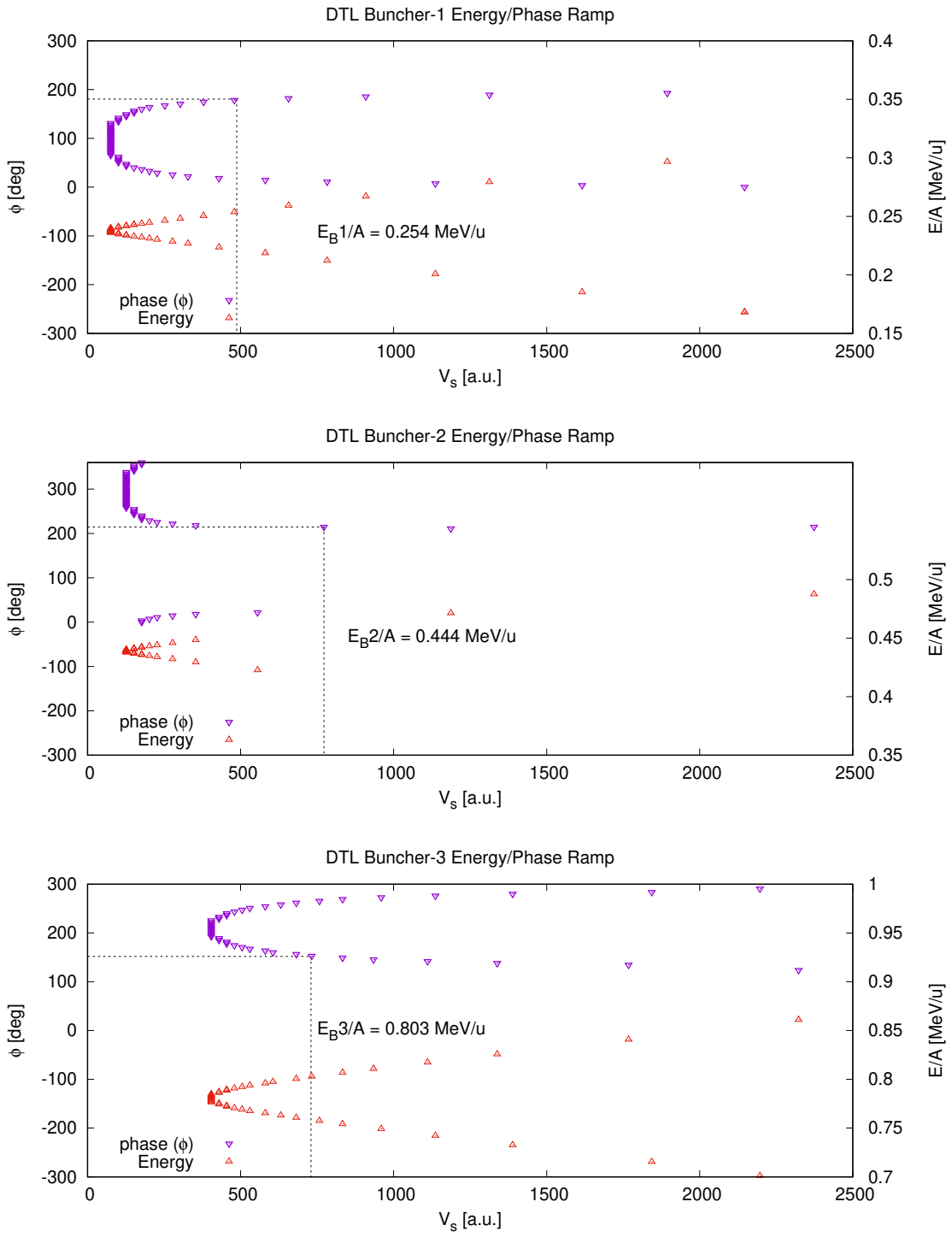

Figure 22: TRANSOPTR Computed DTL Energy-Phase ramps, against EPICS voltage parameter. Note the pure bunching energy, where the energy ramp reverses.

Tank	EPICS V [a.u.]	ϕ [deg]
IH Tank-1	757.6	9.8
Buncher-1	487.5	187.3
IH Tank-2	1051.3	75.1
Buncher-2	772.2	214.5
IH Tank-3	1055.7	257.8
Buncher-3	730.0	152.2
IH Tank-4	1277.4	298.0
IH Tank-5	1550.0	137.5

Table 12: `TRANSOPTR` computed longitudinal tune setpoints for tank voltage and phases, producing tank/buncher energy output as specified in Table 1.

The longitudinal A/q=6 tune in Table 12 was found while completely ignoring the transverse beam parameters. It is also noted that the bunchers here have been set according to the same prescription as the IH tanks, at maximum acceleration, giving a tune which underbunches the beam longitudinally, procuding a longer time-structure while still having a minimized output energy spread. This tune is intended for model development and not operational use, as of yet.

5.3 Transverse ISAC-DTL Envelope

As a demonstration of the optr-DTL's ability to produce ISAC linac tunes, the design tune exiting the MEBT section, at the location of DTL:FC0, has been fed into the ISAC-DTL and flown up to the HEBT1-Prague diagnostic station. Recalling that in Section 4, a set of optr `TWISSMATCH` calls were inserted as element `fortline` in the `/acc` database, automatically being included in `sy.f` for each `xml2optr` generation of the DTL sequence.

An advantage of this database inclusion of transverse focussing calls is that match parameters can easily be loaded into the database, facilitating the adjustment of the tune. Moreover, the constant presence of 8 separate `TWISSMATCH` lines, 2 after each triplet, means each can now be optimized via optr's internal optimizer [24], by enabling the optimize flag in `data.dat` for each triplet. Table 13 shows the Twiss parameters that were used for the present tune generation.

Each triplet has been individually optimized using this method, with the resulting transverse tune shown in Table 14. As a final demonstration of the model, an A/q = 30u/5 tune, with injection energy of 0.153 MeV/u and injection parameters from Tables 11 and 10, is shown in Figure 23, featuring acceleration up to 1.53 MeV/u, corresponding to Tank-5 design output energy.

TWISSMATCH-1		TWISSMATCH-2		TWISSMATCH-3		TWISSMATCH-4	
(α_x, β_x)	(α_y, β_y)	(α_x, β_x)	(α_y, β_y)	(α_x, β_x)	(α_y, β_y)	(α_x, β_x)	(α_y, β_y)
(2.52,91.07)	(1.86,91.72)	(2.32,216.44)	(1.42,98.88)	(0.50,60.25)	(1.28,136.24)	(2.24,195.97)	(0.99,74.74)

Table 13: Loaded DTL transverse Twiss parameters, used for the `TWISSMATCH` statements in `dtl_db0.xml` (Sec. 4), used to define the transverse DTL tune in the present analysis. The parameters are derived from [2]. All Twiss-$\beta_{x,y}$ parameters are in [cm].

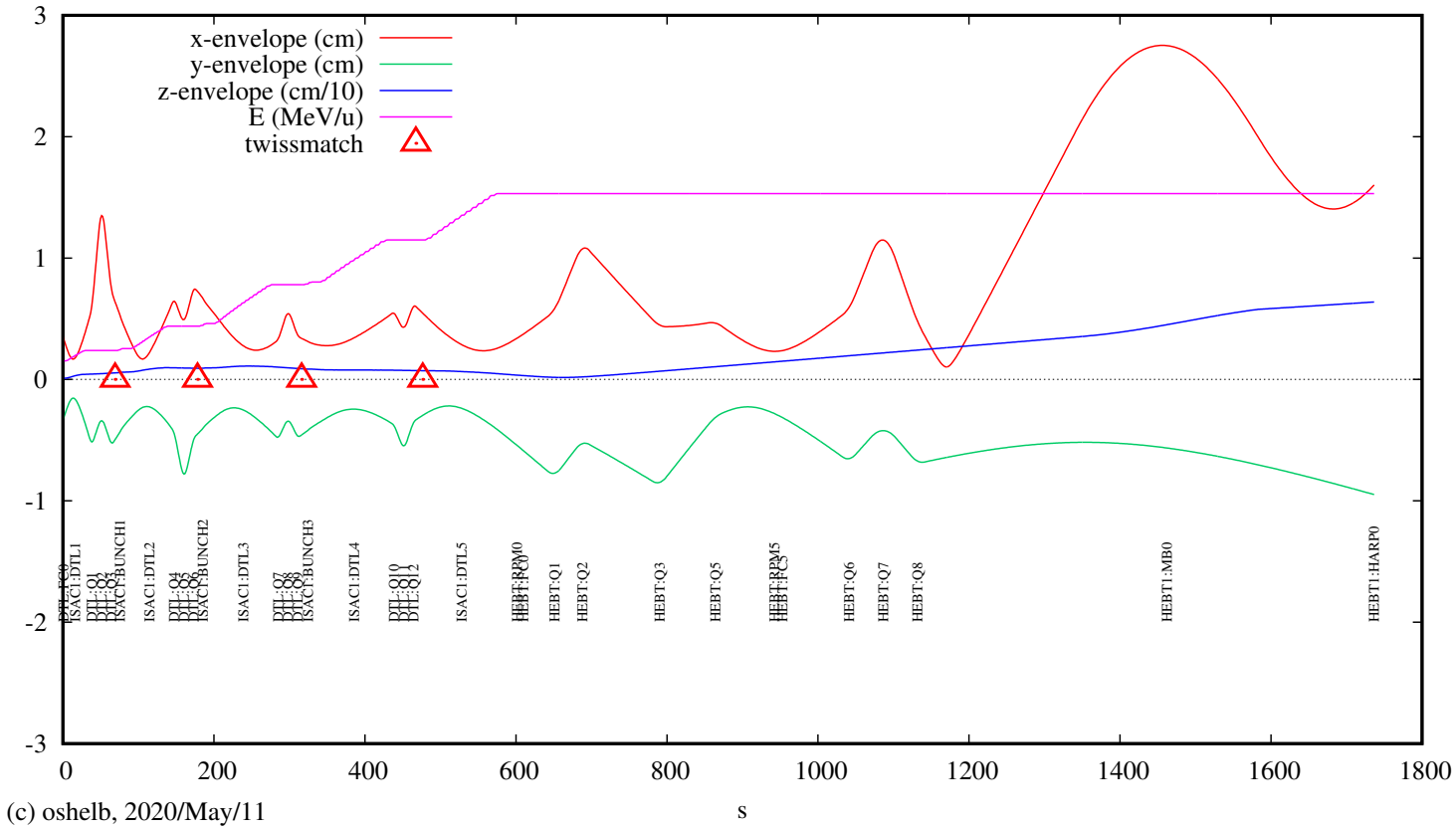

Figure 23: `TRANSOPTR` 2rms ISAC-DTL envelope simulation with Tank-5 output at 1.53 MeV/u, starting at DTL:FC0 and terminating at the HEBT1-Prague Harp energy diagnostic. An A/q = 30u/5 beam is injected at 0.153 MeV/u following design parameters obtained from [9]. Simulation starting parameters shown in Tables 11 & 10 and `TWISSMATCH` parameters from Table 13. The model longitudinal tune is shown in Table 12. Twiss parameter matching point s-coordinates are shown as red triangles.

Quadrupole	Setpoint [A]
DTL:Q1	146.3
DTL:Q2	117.7
DTL:Q3	104.2
DTL:Q4	126.9
DTL:Q5	126.5
DTL:Q6	108.5
DTL:Q7	141.8
DTL:Q8	151.4
DTL:Q9	124.9
DTL:Q10	126.8
DTL:Q11	167.6
DTL:Q12	157.2

Table 14: TRANSOPTR computed DTL quadrupole settings for Tank-5 energy tune from Table 12. Quadrupole BI parametrization found in [15].

6 Conclusion

The TRANSOPTR-DTL presented herein is intended as a tool for research & development, enabling realtime simulation and study of operational tunes and further investigations of machine configuration. Starting from design drawings, tube dimensions and a handful of boundary conditions, the optr model has been built, then used to compute a full longitudinal DTL tune through model analysis. This was then verified against $^{16}O^{4+}$ energy-phase curves, which were also used to generate a calibration between the model and the EPICS control system's voltage variables.

Good agreement between model and machine was found with all cavities, except Tank-3 and Buncher-3. Consideration of the challenging nature of the energy measurement for Tank-3 may at least partially explain this disagreement. For Buncher-3 it was noted that during acquisition the high-energy peak, not the broad body of the energy distribution, was tracked beyond the optimum accelerating phase, producing a systematic disagreement with the optr prediction. While these factors possibly explain some of the discrepancies, from Fig. 14, it is evident that more scrutiny is called for, particularly when considering the degree of agreement for the remainder of the linac. An investigation into the longitudinal dynamics using a multiparticle model in the code LORASR is also underway.

The availability of a full TRANSOPTR end-to-end model for the ISAC-I linac now opens the door to the development of model-coupled accelerator tuning software and techniques, by exploiting the TRIUMF-HLA infrastructure. To this end, the transverse DTL tune will also see more scrutiny.

7 Acknowledgements

In some kind of order, the following people assisted in data acquisition and are all thanked: Tiffany Angus, Spencer Kiy, Justin Lewis and Stephanie Rädel. Were it not for their efforts, it would not have been possible to exploit the available development time fully, depriving this work of such a complete dataset. Sincere gratitude to Oliver Kester, who has been the main driver of the effort to expand tuning capabilities at ISAC, in addition to providing insight and advice during this process. Rick Baartman was of course essential to this work, helping with everything from `TRANSOPTR` operation to conceptual discussions about RF acceleration and beam dynamics. Thanks to Bob Laxdal for patiently searching for DTL source material and providing insight, advice and knowledge on the ISAC DTL. Thomas Planche and Paul Jung have also greatly contributed to this work, in the form of their own hard work toward the development of the HLA platform and also numerous discussions and much advice. The package `xml2optr` has been indispensable for this project. Marco Marchetto is also sincerely thanked for his help, training and assistance throughout this endeavour.

References

[1] RE Laxdal, PG Bricault, T Reis, and DV Gorelov. A separated function drift-tube linac for the isac project at triumf. In *Proceedings of the 1997 Particle Accelerator Conference (Cat. No. 97CH36167)*, volume 1, pages 1194–1196. IEEE, 1997.

[2] R.E. Laxdal. *Concept Design for Quadrupole Triplets for the ISAC Separated Function Drift Tube Linac*. Technical Report TRI-DN-99-05, TRIUMF, 1999.

[3] R. Baartman. Linac Envelope Optics. Technical Report TRI-BN-15-03, TRIUMF, 2015.

[4] O. Shelbaya. ISAC-I RF Acceleration. Technical Report TRI-BN-18-02, TRIUMF, 2018.

[5] M Marchetto, J Berring, and RE Laxdal. Upgrade of the isac dtl tuning procedure at triumf. *EPAC08, Genoa*, page 3440, 2008.

[6] O. Shelbaya. Anomalous Operational OLIS Tunes. Technical Report TRI-BN-19-20, TRIUMF, 2019.

[7] O. Shelbaya. OLIS Maintenance Summary by Oli S. Technical Report TRI-BN-20-04, TRIUMF, 2020.

[8] O Shelbaya, R Baartman, and O Kester. Fast radio frequency quadrupole envelope computation for model based beam tuning. *Physical Review Accelerators and Beams*, 22(11):114602, 2019.

[9] O. Shelbaya. TRANSOPTR Implementation of the MEBT Beamline. Technical Report TRI-BN-19-02, TRIUMF, 2019.

[10] O. Shelbaya. TRANSOPTR Implementation of the HEBT Beamlines. Technical Report TRI-BN-19-06, TRIUMF, 2019.

[11] O. Shelbaya. TRANSOPTR Implementation of ISAC-II. Technical Report TRI-BN-19-13, TRIUMF, 2019.

[12] Spencer Kiy, Olivier Shelbaya, Marco Marchetto, Robert Laxdal, and Stephanie Rädel. Beam-based measurements of the isac-ii superconducting heavy ion linac. 2018.

[13] Olivier Shelbaya, Richard Baartman, Oliver Kester, Spencer Kiy, et al. Toward autonomous phasing of isac heavy ion linacs. In *10th Int. Partile Accelerator Conf.(IPAC'19), Melbourne, Australia, 19-24 May 2019*, pages 3827–3830. JACOW Publishing, Geneva, Switzerland, 2019.

[14] O. Shelbaya. Addition of global time tracking to TRANSOPTR. Technical Report TRI-BN-20-03, TRIUMF, 2020.

[15] O. Shelbaya and R. Baartman. Langevin-Like DTL Triplet BI Fits and Analysis of Transverse DTL Tuning Difficulties. Technical Report TRI-BN-19-18, TRIUMF, 2019.

[16] Barquest C. *Web-Based Control Room Applications at TRIUMF*. In *Proceedings of the 9th International Particle Accelerator Conference*, pages 4832–35, 2018.

[17] DV Gorelov, PN Ostroumov, and RE Laxdal. Use of the lana code for the design of a heavy ion linac. In *Proceedings of the 1997 Particle Accelerator Conference (Cat. No. 97CH36167)*, volume 2, pages 2621–2623. IEEE, 1997.

[18] Vasyuchenko A, Feschenko A, Kvasha A, Menshov A, and Paramonov V et al. *Development, Fabrication and Test of Triple Gap Split-Ring Bunchers for the TRIUMF ISAC Facility*. In *Proceedings of the 2001 Particle Accelerator Conference, Chicago, IL*, pages 978–80, 2001.

[19] Bricault P, Dutto G, R. Laxdal, and et al. Mitra A. *Status Report on the Construction of the ISAC Drift Tube Linac*. In *Proceedings of the XX International Linac Conference, Monterrey, CA*, pages 208–10, 2000.

[20] RE Laxdal, G Dutto, K Fong, G Mackenzie, M Pasini, R Poirier, and R Ruegg. Beam commissioning and first operation of the isac dtl at triumf. In *PACS2001. Proceedings of the 2001 Particle Accelerator Conference (Cat. No. 01CH37268)*, volume 5, pages 3942–3944. IEEE, 2001.

[21] O. Shelbaya. Longitudinal Beam Topology with TRANSOPTR. Technical Report TRI-BN-20-01, TRIUMF, 2020.

[22] O. Shelbaya. Nonlinear RF Cavities. Technical Report TRI-BN-20-05, TRIUMF, 2020.

[23] O. Shelbaya. Cosecant Energy-Phase Ramp for Linear Response RF Cavities. Technical Report TRI-BN-20-07, TRIUMF, 2020.

[24] R. Baartman. `TRANSOPTR`: Changes since 1984. Technical Report TRI-BN-16-06, TRIUMF, 2016.

Appendices

A DTL Energy-Phase Mapping Original Run-Plan

A.1 Run Plan

A systematic approach will ensure consistent data acquisition practices. The OLIS microwave source will produce several nanoamps of 16O+, stripped to 4+ in MEBT. Beam will be tuned from OLIS through the RFQ and MEBT section and initially drifted through the DTL, to be measured on the Prague magnet at the expected 0.153 MeV/u drift energy. Prior to DTL energy phasing investigations, a parasitic test of the RFQ's energy acceptance and output will be performed, providing data for ongoing RFQ modellization efforts. An OLIS emittance scan will also be performed for beam characterization. Following this, the energy-phase investigation of the DTL will carry forward.

This will be accomplished by incrementing DTL tank amplitudes by a fixed amount finding the corresponding maximum accelerating phase. These are noted, then the phase will be scanned on either side of maximum acceleration at constant intervals and the corresponding output energy profile centroid and FWHM recorded. The measurements are to be carried out on each of the five DTL accelerating tanks and its 3 bunchers, providing a mapping of the whole linac.

A.2 Protocol

All required RPM scans should both be graphically saved to the ISAC e-log, and saved as a data file for later analysis. All DTL energy-phase measurements will be logged in a provided run logbook, written in ink.

A.2.1 OLIS Emittance Measurement

1. Tune beam up to the Prague magnet, drifting through the DTL, with the MEBT rebuncher off.
2. Perform an OLIS emittance measurement.

A.2.2 Parasitic RFQ Experiment

Validation of PARMTEQ and TRANSOPTR model performance requires a measurment of the RFQ output transmission and energy for varying input beam energy.

Once beam is tuned through the RFQ following standard practices, the OLIS voltage will be scanned around the input energy. Both the RFQ transmission between ILT:FC49 and MEBT:FC5 will be recorded, in addition to the FWHM and energy centroid on the Prague magnet.

1. Find both the lower and upper source biases that completely kill transmission through the RFQ, as measured on MEBT:FC5.
2. Go to the lower voltage.
3. Increment the source bias by a value equal to one tenth the difference between the low and high injection voltages.
4. For each step, record the RFQ transmission, profile on MEBT:FC5, time profile on MEBT:FFC5 and energy profile on the Prague HARP.

A.2.3 DTL Energy-Phase Mapping

1. Ensure DTL drifting tune is fully optimized using standard practices.
2. Document initial drifting tune through DTL. Scan ILT:RPM37, MEBT:RPM5, HEBT:RPM5, take transmission snapshot and record Prague HARP and beam energy.
3. Turn on DTL Tank1 at EPICS amplitude 400.
4. Reoptimize DTL Quadrupoles, find beam on Prague magnet.
5. Find maximum accelerating phase, take transmission snapshot.
6. With a step size of 10°, record the output energy and FWHM for 10 points below and 10 points above the maximum accelerating phase.
7. Increase Tank amplitude by 50 EPICS units.
8. Repeat from Step 4 until at maximum allowable tank energy.
9. **The last amplitude step should be set to exactly the maximum allowable amplitude.**
10. The above will also be repeated for DTL bunchers.

B TRANSOPTR-DTL sy.f

```
 SUBROUTINE TSYSTEM
 COMMON/SCPARM/QSC,ISC,CMPS
 COMMON/MOM/P,BRHO,pMASS,ENERGK,GSQ,ENERGKi,charge,current
 COMMON/BLOC1/RFA1,RFP1,QM1,QM2,QM3,RFA2,RFP2,RFA3,RFP3,QM4,QM5,QM6
&,RFA4,RFP4,RFA5,RFP5,QM7,QM8,QM9,RFA6,RFP6,RFA7,RFP7,QM10,QM11,QM1
&2,RFA8,RFP8,QM13,QM14,QM15,QM16,QM17,QM18,QM19

 CMPS=1.74   ! Number of cm per step, for plotting only
 wo=1.0 ! Weight aberration from optical elements

 ! start-dtl
 call drift(0.83,".")
 call marker('DTL:FC0')
 call drift(-0.83,".")
 ! RF cavity/linac: ISAC1:DTL1
 call linacn(100,1001,6.79376e-06*RFA1**2.0 - 0.00219132*RFA1 +
&2.55377,32.746,1.0608e+08,1.0*RFP1,'ISAC1:DTL1')
 call drift(2.25875,".")
 ! Magnetic quadrupole DTL:Q1
 call mquad(-213.4777*tanh(1.054896e-24*QM1**5.0 +
&3.599039e-15*QM1**3.0 + 2.210222e-05*QM1),1.1988,6.5,wo,'DTL:Q1')
 call drift(4.99845,".")
 ! Magnetic quadrupole DTL:Q2
 call mquad(251.3987*tanh(5.982539e-25*QM2**5.0 +
&2.560897e-15*QM2**3.0 + 1.9732e-05*QM2),1.1988,9.5,wo,'DTL:Q2')
 call drift(4.95,".")
 ! DTL:XCB2
 ! DTL:YCB2
 call drift(0.04845,".")
 ! Magnetic quadrupole DTL:Q3
 call mquad(-213.4777*tanh(1.054896e-24*QM3**5.0 +
&3.599039e-15*QM3**3.0 + 2.210222e-05*QM3),1.1988,6.5,wo,'DTL:Q3')
 call drift(1.7,".")
 call TWISSMATCH( 1, 2.52,91.07, 0.5, 1)
 call TWISSMATCH( 3, 1.86,91.72, 0.5, 1)
 call drift(-0.004235,".")
 ! RF cavity/linac: ISAC1:BUNCH1
 call linacn(101,1001,0.007986697*RFA2 +
&0.3061407,13.050,1.0608e+08,1.0*RFP2,'ISAC1:BUNCH1')
 call drift(4.85129,".")
 ! RF cavity/linac: ISAC1:DTL2
 call linacn(102,1001,0.006828576*RFA3 -
&0.3663625,54.775,1.0608e+08,1.0*RFP3,'ISAC1:DTL2')
```

```
 call drift(2.19065,".")
 ! Magnetic quadrupole DTL:Q4
 call mquad(213.4777*tanh(1.054896e-24*QM4**5.0 +
&3.599039e-15*QM4**3.0 + 2.210222e-05*QM4),1.1988,6.5,wo,'DTL:Q4')
 call drift(4.9985,".")
 ! Magnetic quadrupole DTL:Q5
 call mquad(-251.3987*tanh(5.982539e-25*QM5**5.0 +
&2.560897e-15*QM5**3.0 + 1.9732e-05*QM5),1.1988,9.5,wo,'DTL:Q5')
 call drift(4.95,".")
 ! DTL:XCB5
 ! DTL:YCB5
 call drift(0.0484,".")
 ! Magnetic quadrupole DTL:Q6
 call mquad(213.4777*tanh(1.054896e-24*QM6**5.0 +
&3.599039e-15*QM6**3.0 + 2.210222e-05*QM6),1.1988,6.5,wo,'DTL:Q6')
 call drift(1.7,".")
 call TWISSMATCH( 1, 2.32,216.44, 0.5, 1)
 call TWISSMATCH( 3, 1.42,98.88, 0.5, 1)
 call drift(-0.002055,".")
 ! RF cavity/linac: ISAC1:BUNCH2
 call linacn(103,1001,-1.5917e-06*RFA4**2.0 + 0.008996733*RFA4 -
&0.718549,14.850,1.0608e+08,1.0*RFP4,'ISAC1:BUNCH2')
 call drift(4.84989,".")
 ! RF cavity/linac: ISAC1:DTL3
 call linacn(104,1001,0.007007824*RFA5 -
&0.4691255,81.775,1.0608e+08,1.0*RFP5,'ISAC1:DTL3')
 call drift(2.19195,".")
 ! Magnetic quadrupole DTL:Q7
 call mquad(-213.4777*tanh(1.054896e-24*QM7**5.0 +
&3.599039e-15*QM7**3.0 + 2.210222e-05*QM7),1.1988,6.5,wo,'DTL:Q7')
 call drift(4.9984,".")
 ! Magnetic quadrupole DTL:Q8
 call mquad(251.3987*tanh(5.982539e-25*QM8**5.0 +
&2.560897e-15*QM8**3.0 + 1.9732e-05*QM8),1.1988,9.5,wo,'DTL:Q8')
 call drift(4.95,".")
 ! DTL:XCB8
 ! DTL:YCB8
 call drift(0.0485,".")
 ! Magnetic quadrupole DTL:Q9
 call mquad(-213.4777*tanh(1.054896e-24*QM9**5.0 +
&3.599039e-15*QM9**3.0 + 2.210222e-05*QM9),1.1988,6.5,wo,'DTL:Q9')
 call drift(1.7,".")
 call TWISSMATCH( 1, 0.50,60.25, 0.5, 1)
 call TWISSMATCH( 3, 1.28,136.24, 0.5, 1)
 call drift(-0.00209,".")
 ! RF cavity/linac: ISAC1:BUNCH3
```

```
 call linacn(105,1001,0.006496419*RFA6 +
&0.1508214,17.349,1.0608e+08,1.0*RFP6,'ISAC1:BUNCH3')
 call drift(4.8499,".")
 ! RF cavity/linac: ISAC1:DTL4
 call linacn(106,1001,0.004845639*RFA7 -
&0.1695915,94.775,1.0608e+08,1.0*RFP7,'ISAC1:DTL4')
 call drift(2.19189,".")
 ! Magnetic quadrupole DTL:Q10
 call mquad(213.4777*tanh(1.054896e-24*QM10**5.0 +
&3.599039e-15*QM10**3.0 +
&2.210222e-05*QM10),1.1988,6.5,wo,'DTL:Q10')
 call drift(4.9985,".")
 ! Magnetic quadrupole DTL:Q11
 call mquad(-251.3987*tanh(5.982539e-25*QM11**5.0 +
&2.560897e-15*QM11**3.0 + 1.9732e-05*QM11),1.1988,9.5,wo,'DTL:Q11')
 call drift(4.95,".")
 ! DTL:XCB11
 ! DTL:YCB11
 call drift(0.0484,".")
 ! Magnetic quadrupole DTL:Q12
 call mquad(213.4777*tanh(1.054896e-24*QM12**5.0 +
&3.599039e-15*QM12**3.0 +
&2.210222e-05*QM12),1.1988,6.5,wo,'DTL:Q12')
 call drift(8.8656,".")
 call TWISSMATCH( 1, 2.24,195.97, 0.5, 1)
 call TWISSMATCH( 3, 0.99,74.74, 0.5, 1)
 ! RF cavity/linac: ISAC1:DTL5
 call linacn(107,1001,1e-06*RFA8,102.77,1.0608e+08,1.0*RFP8,'ISAC1:
&DTL5')
 ! endOf_dtl_db0
 call drift(6.4599,".")
 ! startOf_t3d_tune_hebt
 call drift(5.7751,".")
 ! HEBT:IV0
 call drift(9.785,".")
 call marker('HEBT:RPM0')
 call drift(8.262,".")
 call marker('HEBT:FC0')
 call drift(20.678,".")
 ! HEBT:XCB0
 ! HEBT:YCB0
 call drift(11.5,".")
 ! Magnetic quadrupole HEBT:Q1
 call mquad(-0.009228503*QM13,2.6,18.0,wo,'HEBT:Q1')
 call drift(19.0,".")
 ! Magnetic quadrupole HEBT:Q2
```

```
call mquad(0.009228503*QM14,2.6,18.0,wo,'HEBT:Q2')
call drift(72.977,".")
! HEBT:XCB2
! HEBT:YCB2
call drift(11.523,".")
! Magnetic quadrupole HEBT:Q3
call mquad(-0.009228503*QM15,2.6,18.0,wo,'HEBT:Q3')
call drift(56.0,".")
! Magnetic quadrupole HEBT:Q5
call mquad(0.009228503*QM16,2.6,18.0,wo,'HEBT:Q5')
call drift(69.0,".")
call marker('HEBT:RPM5')
! HEBT:STRP5
call drift(10.54,".")
call marker('HEBT:FC5')
! HEBT:SCD5
call drift(15.129,".")
! HEBT:PSID5
call drift(12.914,".")
! HEBT:IV8
call drift(37.274,".")
! HEBT:XCB5
! HEBT:YCB5
call drift(14.143,".")
! Magnetic quadrupole HEBT:Q6
call mquad(-0.009283983*QM17,2.6,18.0,wo,'HEBT:Q6')
call drift(20.0,".")
! Magnetic quadrupole HEBT:Q7
call mquad(0.009477347*QM18,2.6,32.5,wo,'HEBT:Q7')
call drift(20.0,".")
! Magnetic quadrupole HEBT:Q8
call mquad(-0.009228503*QM19,2.6,18.0,wo,'HEBT:Q8')
call drift(13.46,".")
! HEBT:XCB8
! HEBT:YCB8
call drift(10.08,".")
! HEBT:XCOL8A
call drift(9.8153,".")
! endOf_hebt_db0
call drift(167.162,".")
! Magnetic dipole HEBT1:MB0
call edge(0.0,153.719,90.0,0.0,0.0,0.0,5.0,0.0,wo)
call bend(153.719,90.0,0.0,'HEBT1:MB0')
call edge(0.0,153.719,90.0,0.0,0.0,0.0,5.0,0.0,wo)
call drift(86.143,".")
! HEBT1:IV0
```

```
call drift(67.3875,".")
call marker('HEBT1:HARP0')
call print_transfer_matrix
return
end
```

C TRANSOPTR-DTL data.dat

```
4.59 0.0 0.0 27944.8 5.0 0.0 ! En[MeV], mom., brho, mass[MeV], charge, beam cur. or bun.chg.
-1 5 0.01 0.0001 ! iprint, IVOPT (4/5: 4/6-D space-charge), initial RK step, RK error tol.
0 0.0 1.0 0.0 ! for external Bs (0=disable), s offset, unit of s (1=cm), unit of Bs (1=kG)
0.358748 0.0236304 0.34 0.0225397 0.1345 0.025171 ! bunch dim: x,x',y,y',z(bun. len.),dp/p
1.0 1.0 1.0 1.0 1.0 1.0 1.0 1.0 ! 1 means x,y,z in cm, x',y',dp/p in rad (dimensionless)
3
1 2 -0.887894 3 4 -0.896195 5 6 -0.62
35
757.58     0.0        2500.0     0 ! ISAC1:DTL1:AMP:SETPT RFA1 V
10.0       -360.0     360.0      0 ! ISAC1:DTL1:PHASE:SETPT RFP1 deg
129.1      0.0        250.0      0 ! DTL:Q1:CUR QM1 A
111.1      0.0        250.0      0 ! DTL:Q2:CUR QM2 A
99.26      0.0        250.0      0 ! DTL:Q3:CUR QM3 A
487.48     -38.33     2500.0     0 ! ISAC1:BUNCH1:AMP:SETPT RFA2 V
187.34     -360.0     360.0      0 ! ISAC1:BUNCH1:PHASE:SETPT RFP2 deg
1051.28    0.0        2500.0     0 ! ISAC1:DTL2:AMP:SETPT RFA3 V
75.14      -360.0     360.0      0 ! ISAC1:DTL2:PHASE:SETPT RFP3 deg
109.7      0.0        250.0      0 ! DTL:Q4:CUR QM4 A
119.5      0.0        250.0      0 ! DTL:Q5:CUR QM5 A
102.9      0.0        250.0      0 ! DTL:Q6:CUR QM6 A
772.15     0.0        2500.0     0 ! ISAC1:BUNCH2:AMP:SETPT RFA4 V
214.53     -360.0     360.0      0 ! ISAC1:BUNCH2:PHASE:SETPT RFP4 deg
1055.7     0.0        2500.0     0 ! ISAC1:DTL3:AMP:SETPT RFA5 V
257.84     -360.0     360.0      0 ! ISAC1:DTL3:PHASE:SETPT RFP5 deg
134.9      0.0        250.0      0 ! DTL:Q7:CUR QM7 A
147.3      0.0        250.0      0 ! DTL:Q8:CUR QM8 A
112.8      0.0        250.0      0 ! DTL:Q9:CUR QM9 A
613.58     -23.22     2500.0     0 ! ISAC1:BUNCH3:AMP:SETPT RFA6 V
124.17     -360.0     360.0      0 ! ISAC1:BUNCH3:PHASE:SETPT RFP6 deg
1277.35    0.0        2500.0     0 ! ISAC1:DTL4:AMP:SETPT RFA7 V
303.33     -360.0     360.0      0 ! ISAC1:DTL4:PHASE:SETPT RFP7 deg
121.3      0.0        250.0      0 ! DTL:Q10:CUR QM10 A
156.4      0.0        250.0      0 ! DTL:Q11:CUR QM11 A
134.6      0.0        250.0      0 ! DTL:Q12:CUR QM12 A
0.0        0.0        2e+08      0 ! ISAC1:DTL5:AMP:SETPT RFA8 V
```

```
0.0         -360.0      360.0       0 ! ISAC1:DTL5:PHASE:SETPT RFP8 deg
25.5712     0.0         60.0        0 ! HEBT:Q1:CUR QM13 A
30.4147     0.0         60.0        0 ! HEBT:Q2:CUR QM14 A
20.1343     0.0         60.0        0 ! HEBT:Q3:CUR QM15 A
18.3696     0.0         60.0        0 ! HEBT:Q5:CUR QM16 A
25.7267     0.0         60.0        0 ! HEBT:Q6:CUR QM17 A
23.8863     0.0         60.0        0 ! HEBT:Q7:CUR QM18 A
18.9906     0.0         60.0        0 ! HEBT:Q8:CUR QM19 A
0.001 20
10 0.0 0.95 20
```